Article

Flavonoid Derivatives as New Potent Inhibitors of Cysteine Proteases: An Important Step toward the Design of New Compounds for the Treatment of Leishmaniasis

Estela Mariana Guimarães Lourenço[1], Juliana Fortes Di Iório[2], Fernanda da Silva[3], Felipe Leonardo Bley Fialho[1], Melquisedeque Mateus Monteiro[4], Adilson Beatriz[1], Renata Trentin Perdomo[4], Euzébio Guimarães Barbosa[5], Jean Pierre Oses,[6] Carla Cardozo Pinto de Arruda[3], Wagner Alves de Souza Júdice[2,*], Jamal Rafique[1,*], Dênis Pires de Lima[1,*]

[1] Laboratory of Synthesis and Transformation of Organic Molecules - SINTMOL, Institute of Chemistry, Universidade Federal de Mato Grosso do Sul, Av. Senador Filinto Muller, 1555, Campo Grande, MS, Brazil
[2] Centro Interdisciplinar de Investigação Bioquímica (CIIB), Universidade de Mogi das Cruzes (UMC), Mogi das Cruzes, SP, Brazil
[3] Laboratório de Parasitologia Humana, Instituto de Biociências, Universidade Federal de Mato Grosso do Sul, Campo Grande, MS, Brazil
[4] Laboratory of Molecular Biology and Cell Culture, School of Pharmaceutical Sciences, Food Technology, and Nutrition, Universidade Federal de Mato Grosso do Sul, Campo Grande, MS, Brazil
[5] Laboratório de Química Farmacêutica Computacional, Departamento de Farmácia, Universidade Federal do Rio Grande do Norte, Natal, Brazil
[6] Laboratório de Neurociências, Instituto de Biociências, Universidade Federal do Rio Grande, Rio Grande, RS, Brazil.
* Correspondence: wagnerjudice@gmail.com (WASJ); jamal.chm@gmail.com; jamal.rafique@ufms.br (JR); denis.lima@ufms.br (DPL)

Abstract: Leishmaniasis is a neglected tropical disease and affects more than 350 million people worldwide. However, there are no vaccines for humans, and current treatment is hampered due to its high cost, numerous side effects, and painful administration routes. Ending its epidemics by 2030 has become a United Nations goal, and the multitarget drug strategy emerges as a promising alternative. Flavonoids are an example of multitarget compounds and organic synthesis represents a tool to obtain high yields of these molecules. In our study, we synthesized 17 flavonoid analogs using a scalable, easy-to-reproduce, and inexpensive method. All compounds demonstrated an impressive inhibition capacity against rCPB2.8, rCPB3, and rH84Y, which are highly expressed in the amastigote stage, the target form of the parasite. Compounds **3c**, **f12a**, and **f12b** stood out as effective against all isoforms and intermolecular interactions were investigated through a molecular modeling study. The compounds were highly potent against the parasite and demonstrated low cytotoxic action against mammalian cells. The results were pioneering, representing an advance in the investigation of the mechanisms behind the antileishmanial action of flavonoid derivatives. Furthermore, compounds have shown to be promising leads for the design of other cysteine protease inhibitors for the treatment of leishmaniasis diseases.

Keywords: synthesis; leishmaniasis; flavonoids; rCPB; molecular modelling.

1. Introduction

Leishmaniasis comprises a group of vector-borne infectious diseases with a broad clinical spectrum. Classified as a neglected disease by the World Health Organization (WHO), leishmaniasis affects more than 350 million people worldwide [1,2]. Although it represents a serious public health problem, there is still no vaccine for humans. In addition, the drugs used in therapy are expensive and highly toxic, cause numerous side effects, and the routes of administration are painful. Consequently, adherence to treatment is impaired, further strengthening the disease cycle, especially in developing countries [3].

 doi:10.20944/preprints202211.0376.v1

The serious situation involving Leishmaniasis made combating this group of diseases a goal of the United Nations (UN) in 2020. Sustainable Development Goal (SDG) 3.3 aims to end the epidemics of several diseases, including Neglected Tropical Diseases (NTDs) by 2030 [4]. This objective has made the discovery and development of new antileishmanial drugs that are more effective, cheaper, easily obtainable and capable of being administered by alternative routes an emergency. To achieve this goal, different drug discovery approaches need to be used. Between them, the multitarget drug strategy has emerged in the last decades. This approach is based on the complexity of the pathologies and considers that single-target drugs are insufficient to achieve the desired therapeutic effects [5]. Recently, the multitarget drug strategy was reported as a tool to accelerate the discovery of safer, more active, and patient-compliant drugs for the treatment of leishmaniasis [6].

In countries rich in biodiversity such as Brazil, the use of secondary metabolites from natural sources as new prototypes is a compelling alternative. Flavonoids stand out for comprising one of the most diverse groups of secondary metabolites, marked by their wide distribution in plants and different therapeutic potentials [7]. These compounds are structurally versatile due to their chemical core and are considered important prototypes for the development of multi-target drugs (**Figure 1**). It is essential to note that flavonoids have shown in vitro and in vivo antileishmanial activity [8,9]. Flavonols such as quercetin and fisetin inhibit the arginase enzyme, as well as modulate the host's immune response against the parasite, resulting in low patient toxicity [8]. However, the process of isolating and purifying these compounds is expensive and time-consuming. These methodologies generally require high-cost equipment, result in low yield, and use toxic solvents, which reduces the sustainability of the process.

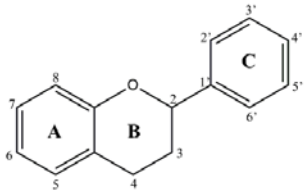

Figure 1: Chemical flavonoid core (C6-C3-C6)

In line with our interest in discovering and developing a new sustainable, efficient methodologies for biologically active compounds and patient-compliant alternative for leishmaniasis treatment [10-17], our research group aimed to yield natural-based bioactive compounds with multitarget properties. To achieve this purpose, we designed a scalable, easy-to-replicate, and inexpensive synthetic route to obtain flavonol and chalcone analogs. The antileishmanial activity was elucidated by in vitro and in silico methods, and the cytotoxicity was measured to determine the Selectivity Index.

2. Results and discussion

2.1. Chemistry

Our retrosynthetic analysis was based on green chemistry principles. Thus, we used mild reaction conditions and inexpensive catalysts and reagents (**Figure 2**). Chalcone analogue synthesis consists of a Claisen-Schmidt reaction that is a condensation of aldehydes and carbonyl compounds leading to α, β-unsaturated ketones in the presence of a base or Lewis acid [18]. In particular, the use of a base as a catalyst provides higher yields for obtaining flavonol-like compounds. The intramolecular H-bond of o-hydroxyacetophenones leads to an increase in acidity of its α-hydrogen and, in the presence of a base, aids in the generation of a strongly attacking enol anion [19]. Chalcone analogs were used in the synthesis of flavonol-like molecules through the Algar Flynn-Oyamada reaction, in which a chalcone undergoes an oxidative cyclization under alkaline conditions to form a flavonol [20].

Preprints (www.preprints.org) | NOT PEER-REVIEWED | Posted: 21 November 2022 doi:10.20944/preprints202211.0376.v1

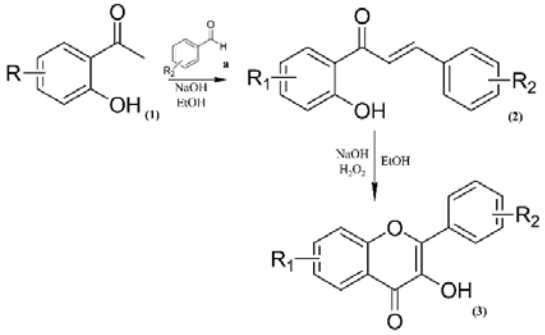

Figure 2: Synthetic route to obtain flavonol-like compounds

To obtain inexpensive bioactive compounds, we selected low-cost benzaldehydes and acetophenones. The number of synthetic compounds and the structural variations were designed to be statistically relevant for the elucidation of the Structure-Activity Relationship (SAR). Between acetophenones, we also used halogenated o-hydroxyacetophenones, as these substituents are reported for their high and selective antimicrobial actions, including antileishmanial activity [21,22]. The aspects of the synthetic process described previously were reviewed to obtain moderate to high yields of the target compounds (**Table 1**). Our protocol can also be applied to significantly larger reaction mixtures, and this scale-up also gives good yields.

Table 1: Reaction yields of chalcone and flavonol-like compounds

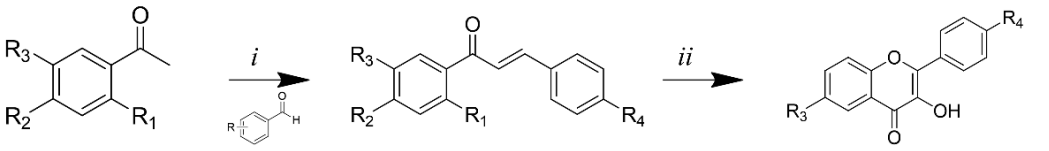

Chalcones 1a-4c | **Flavonol-like compounds** F12a-F13c

Entry	R_1	R_2	R_3	R_4	Yield (%)
1	H	Cl	H	-OCH_3	67.11 (1a)
2	H	Cl	H	-OCH_2O	86.19 (1b)
3	H	Cl	H	-$N(CH_3)_2$	73.26 (1c)
4	OH	H	H	-OCH_3	76.26 (2a)
5	OH	H	H	-OCH_2O	71.43 (2b)
6	OH	H	H	-$N(CH_3)_2$	82.34 (2c)
7	OH	H	Cl	-OCH_3	90.40 (3a)
8	OH	H	Cl	-OCH_2O	86.70 (3b)
9	OH	H	Cl	-$N(CH_3)_2$	81.74 (3c)
10	OH	H	F	-OCH_3	84.32 (4a)
11	OH	H	F	-OCH_2O	76.51 (4b)
12	OH	H	F	-$N(CH_3)_2$	95.69 (4c)
13	-	H	H	-OCH_3	71.34 (f12a)
14	-	H	H	-OCH_2O	69.87 (f12b)
15	-	H	H	-$N(CH_3)_2$	79.40 (f12c)
16	-	H	Cl	-OCH_3	86.42 (f13a)
17	-	H	Cl	-$N(CH_3)_2$	78.67 (f13c)

i: NaOH (3 M), EtOH (dry); *ii*: H_2O_2/NaOH (3M), EtOH (dry);

Higher yields of chalones were achieved when halogenated *o*-hydroxyacetophenones were used. Substituting a halogen atom in the phenolic ring results in an increase

 doi:10.20944/preprints202211.0376.v1

in the acidity of the hydroxyl group, which further favors the formation of the enol anion over the formation of unsubstituted *o*-hydroxyacetophenones [23]. Although chalcones exist as trans (*E*) or cis (*Z*) isomers, the *E* isomer is more stable from the perspective of thermodynamics [24]. The configuration of the *Z* isomer is unstable as a result of the strong steric effects between the carbonyl group and the A-ring, making the *E* isomer the predominant configuration obtained in our study.

The compounds were unambiguously characterized by NMR spectra. Chacones **4a-4c** presented most of the ^{13}C NMR signals as doublets due to the coupling of ^{1}J, ^{2}J and ^{3}J fluorine (spin ½) coupling with the respective carbons in the aromatic ring. Compared to starting materials, the chalcones present signals of CH groups in 7.30 - 7.90 ppm with coupling constants (*J*) of 15.3 Hz, confirming the formation of the *E* isomer. These signals were not observed in the flavonol spectra. Furthermore, compounds **f12a-f13c** presented a signal of the OH group in 9.60 - 9.30, indicating the loss of 2-hydroxy from their starting material (chalcone), classically observed in larger chemical shift due to the intramolecular H bond with the carbonyl group. The NMR data was compared with those of the literature and the structures of the synthesized compounds were confirmed [25-37]. The spectra are available in the Supplementary material.

2.2. Determination of IC50, mechanism of cysteine protease inhibition and evaluation of Structure-Activity Relationship (SAR)

The discovery and development of new antileishmanial drugs are usually directed through phenotypic or target-based approaches [2]. The target-based strategy is based on previous evidence of the action of compounds on specific pharmacological targets. Driven by advances in molecular biology and the urgency to discover new effective drugs, this approach has been the dominant tool in the last three decades [38]. However, most of the molecules designed by the target-based strategy demonstrated only antipromastigote effects, although amastigote is the target form of the parasite, since this stage occurs in mammalian host cells [39].

Leishmania proteases stand out in this context. In particular, cysteine protease B (CPB) expression is elevated in the amastigote stage and plays an important role in the interaction between the parasite and its mammalian host [40]. Inhibition of these proteases generates results that indicate their influence on macrophage infection, amastigote survival in host cells, as well as modulating the host's immune response [41]. The isolated bioflavonoids and their semi-synthetic derivatives demonstrated satisfactory activity against the isoforms rCPB2.8 and rCPB3 [42]. Therefore, these enzymes represent promising therapeutic targets for our study.

Among the chalcones (**1a-4c**) evaluated on rCPB2.8 (**Figure 3A**), the compounds **1a** and **1c** stood out for inhibiting 82.02% of enzymatic activity at 1 μM and 91.59% at 5 μM. The compound **f12b**, which reduced the activity by 69.19% and 77.49% at 1 μM and 5 μM, respectively was the most effective compound in inhibiting rCPB2.8 among flavonols (**f12a-f13c**). Interestingly, chalcone **2c** increased activity to 141.71% at 1 μM but reduced by 25.58% at 5 μM.

In the screening of compounds in rCPB3, it was found that chalcone analogs **1b**, **2a** and **2b** reduced enzymatic activity by 67.01%, 70.92% and 62.55%, respectively, at a concentration of 5 μM. Flavonols, at concentrations of 1 μM or 5 μM were unable to inhibit the enzyme by more than 50% (**Figure 3B**). In inhibition of rH84Y with compounds at 5 μM, it was observed that chalcones **1b**, **1c** and **2c** reduced activity by 73.61%, 82.29% and 70.77%, respectively, while the flavonoid **f12c** reduced activity by 56%. Only compound **2c** was able to inhibit more than 50% at 1 μM (**Figure 3C**).

Since all chalcones and flavonol analogs inhibited the three enzymes to some degree at a concentration of 5 μM, all were subjected to assays to determine their inhibitory potential (IC_{50}) against rCPB2.8 and isoforms.

Preprints (www.preprints.org) | NOT PEER-REVIEWED | Posted: 21 November 2022 doi:10.20944/preprints202211.0376.v1

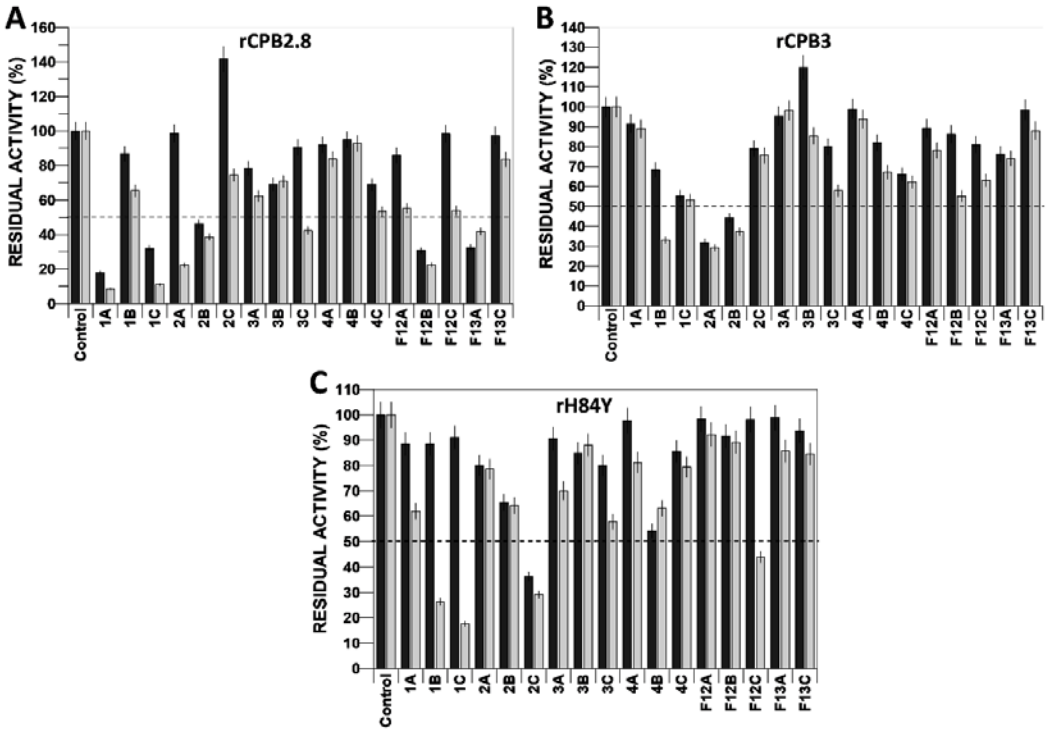

Figure 3: Screening of the action of compounds derived from chalcones and flavonoids on the enzymatic activity of the cysteine protease type B rCPB2.8 of L. mexicana and its isoforms rCPB3 and rH84Y. Black column: 1 μM compound; gray column: 5 μM compound. Dotted line: delimits residual activity by 50%.

The chalcones with the best inhibitory potential in rCPB2.8 were **1c** (IC_{50} = 2.75 ± 0.18 μM), **2a** (IC_{50} = 2.35 ± 0.19 μM), **3c** (IC_{50} = 3.97 ± 0.08 μM) and **4a** (IC_{50} = 3.35 ± 0.17 μM). The presence of chlorine attached on carbon C3' or C4', fluoride on the C3' or hydroxyl on the C6' seems not to affect the inhibitory capacity of the compounds. However, the presence of the1,3-dioxolane group, in general, did not favour enzyme inhibition, as observed for **2b**, which was 8.78 times less efficient in inhibiting rCPB2. 8 times than compound **2a** (**Table 2**).

In inhibition of rCPB3, compounds **1b** (IC_{50} = 5.60 ± 0.35 μM), **3a** (IC_{50} = 4.22 ± 0.81 μM), **3c** (IC_{50} = 5.47 ± 0.59 μM) and **4a** (IC_{50} = 4.51 ± 0.19 μM) showed the best inhibitory potentials among the analogs of chalcones. Compounds bearing chlorine atom at C3' (**3a** and **3c**) or methoxy group at C4 (**3a** and **4a**) had the lowest IC_{50}. On the contrary, the compound with the lower IC_{50} over rCPB3 was **4c** (IC_{50} = 37.97 ± 7.24 μM), which has fluoride, hydroxyl and dimethylamine groups at C3', C6' and C4, respectively (**Table 2**). Chalcones **2b** (IC_{50} = 4.67 ± 0.13 μM), **3c** (IC_{50} = 5.47 ± 0.59 μM) and **4c** (IC_{50} = 4.34 ± 0.43 μM) showed the best inhibitory potentials for rH84Y. Compound **4c** was more efficient in inhibiting rH84Y compared to rCPB2.8 and rCPB3 (**Table 2**).

The difference in amino acid sequence may have affected the inhibitory potential of **4c**. The enzyme rH84Y differs from rCPB3 by a single amino acid residue [43]. Since **4c** was 8.74 times more potent in inhibiting rH84Y compared to rCPB3, it is possible to infer that the substitution of histidine for tyrosine was the variation that most affected the inhibitory potential of **4c**.

Preprints (www.preprints.org) | NOT PEER-REVIEWED | Posted: 21 November 2022 doi:10.20944/preprints202211.0376.v1

Table 2: Chalcone inhibitory potential (IC_{50}) of chalcones to modulate the enzyme activity of Leishmania mexicana cysteine proteases rCPB2.8, rCPB3 and rH84Y.

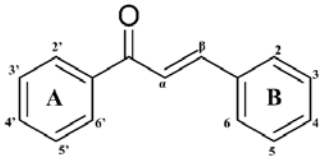

Entry	Compound	IC_{50} (μM)		
		rCPB2.8	rCPB3	rH84Y
1	**1a**	13.66 ± 0.74	9.91 ± 0.59	29.74 ± 2.62
2	**1b**	7.42 ± 0.25	5.60 ± 0.35	15.34 ± 0.60
3	**1c**	2.75 ± 0.18	10.17 ± 0.52	11.70 ± 1.27
4	**2a**	2.35 ± 0.19	7.14 ± 0.86	16.34 ± 0.46
5	**2b**	20.63 ± 1.06	10.99 ± 0.40	4.67 ± 0.13
6	**2c**	11.74 ± 0.38	8.96 ± 0.61	9.90 ± 0.48
7	**3a**	7.11 ± 0.32	4.22 ± 0.81	6.84 ± 0.26
8	**3b**	18.37 ± 1.22	11.56 ± 0.77	8.23 ± 0.21
9	**3c**	3.97 ± 0.08	5.47 ± 0.59	4.81 ± 0.32
10	**4a**	3.35 ± 0.17	4.51 ± 0.19	20.34 ± 1.78
11	**4b**	6.61 ± 0.41	17.27 ± 1.46	7.77 ± 0.72
12	**4c**	9.88 ± 0.73	37.97 ± 7.24	4.34 ± 0.43

In the evaluation of the inhibitory capacity of flavonoids against rCPB2.8, the compounds **f12a** (IC_{50} = 4.72 ± 0.38 μM), **f12b** (IC_{50} = 5.23 ± 0.32 μM) and **f13a** (IC_{50} = 1.86 ± 0.07 μM) showed the highest inhibitory potentials. Methoxy added to the C4' carbon in the **f13a** structure seems to potentiate the enzyme inhibition. On the other hand, the presence of dimethylamine on C4' in **f13c** disfavoured inhibition of rCPB2.8 by 7.62-fold. The compounds **f12a** (IC_{50} = 7.71 ± 0.78 μM) and **f12b** (IC_{50} = 7.06 ± 0.63 μM) showed the best IC_{50} values on rCPB3. Again, it was found that the presence of dimethylamine did not favor rCPB3 inhibition, as the compounds **f12c** (IC_{50}=16.67 ± 2.53 μM) and **f13c** (IC_{50} = 29.75 ± 2.08 μM) were the least effective. Regarding the inhibition of rH84Y, the flavonoids **f12a** (IC_{50} = 3.85 ± 0.27 μM) and **f12b** (IC_{50} = 8.85 ± 0.33 μM) presented the best inhibitory potentials and the compounds **f12c** and **f13c** had the lowest inhibitory capacity (**Table 3**). On the basis of these data, it is observed that the presence of dimethylamine on C4' carbon negatively impacts the inhibition of the three enzymes.

Table 3: Flavonol-like inhibition potential (IC_{50}) in modulating the enzyme activity of Leishmania mexicana cysteine proteases rCPB2.8, rCPB3, and rH84Y..

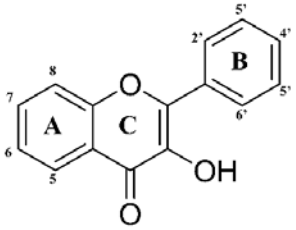

Entry	Compound	IC_{50} (μM)		
		rCPB2.8	rCPB3	rH84Y
13	**f12a**	4.72 ± 0.38	7.71 ± 0.78	3.85 ± 0.27
14	**f12b**	5.23 ± 0.32	7.06 ± 0.63	8.85 ± 0.33
15	**f12c**	10.32 ± 0.39	16.67 ± 2.53	28.56 ± 1.62
16	**f12a**	1.88 ± 0.07	10.56 ± 1.11	11.71 ± 1.54
17	**f13c**	14.18 ± 0.65	29.75 ± 2.08	20.35 ± 1.02

 doi:10.20944/preprints202211.0376.v1

The high inhibition capacity of all compounds against the three enzyme isoforms confirms their multitarget properties. Studies have shown the formation of larger lesions in Balb/c mice that received amastigotes expressing only CPB2.8 compared to those with amastigotes deficient in all three isoforms [44]. This result confirms that inhibition against the three isoforms is essential to developing a new effective antileishmanial compound based on the inhibition of the CPB enzymes. Between the compounds under study, chalcone **3c** and flavonols **f12a** and **f12b** were the most effective simultaneously against all enzymes tested, making them good candidates for prototypes. Therefore, these compounds were selected to evaluate inhibition mechanisms of rCPB2.8, rCPB3, and rH84Y.

By evaluating the inhibition mechanisms of compounds **3c**, **f12a** and **f12b** on rCPB2.8, we verified the slope *vs.* [Inhibitor] and the intercept *vs.* [Inhibitor] (**Figures S1D, S2D, S3D**, Supplementary material) of the parabolic profile. This means that in the inhibition mechanism, two molecules participate in the process. Initially, there will be the binding of the first molecule, which may favour or impair the binding of the second. Respectively, this molecular behaviour is responsible for establishing cooperativity as positive or negative. To determine the affinity constants of the compounds, it was necessary to perform the linearization of the parabolas, obtaining the replots $1/K_{Slope}$ vs [Inhibitor] (**Figures S1E, S2E, S3E**, Supplementary material), $1/K_{Intercept}$ vs [Inhibitor] (**Figures S1F, S2F, S3F**, Supplementary material) and the factors α, β and γ.

According to the replots $1/K_{Slope}$ vs [**3c**] (**Figure 1E**, Supplementary material) and $1/K_{Intercept}$ vs [**3c**] (**Figure S1F**, supplementary material) it was possible to determine the inhibition constants, K_i = 100 ± 18 μM, αK_i = 147 ± 28 μM, βK_i = 0.55 ± 0,10 μM and γK_i = 1.15 ± 0.21 μM. Factor α =1.47 shows that molecule **3c** has a greater preference to bind to the free enzyme. The factors β = 0.0055 and γ = 0.0115 show that binding of the first molecule to form EI or ESI favored 182 and 87-fold the formation of IEI and IESI, respectively (**Table 4**).

The results of the inhibitory mechanism of rCPB2.8 by **f12a** demonstrated a cooperativity inhibition as a function of parabolic replots. Their respective linearization (**Figures S2C, S2D, S2E** and **S2F**, Supplementary material) allowed the determination of K_i = 12.4 ± 1.4 μM and αK_i = 10.7 ± 1.1 μM, being α~1, considering the standard deviation. The first molecule of **f12a** has the same affinity for binding to the free enzyme E or the ES complex. The values of βK_i = 3.65 ± 0.39 μM and γK_i = 0.25 ± 0.03 μM defined β = 0.29 and γ = 0.02 (**Table 4**). Therefore, binding of the first molecule favours the formation of the IEI and IESI complexes 3.4 and 50-fold, respectively.

In inhibition of rCPB2.8 by the compound **f12b** (**Figure S3**, Supplementary material), the values of the constants K_i = 39.2 ± 4.1 μM, αK_i = 24.9 ± 2.3 μM, βK_i = 1.17 ± 0.12 μM and γK_i = 0.51 ± 0.09 μM were calculated. Based on these results, α = 0.634, β = 0.029 and γ = 0.013 were measured (**Table 4**). The data show that the binding of the first **f12a** facilitated the formation of IEI 34-fold and the formation of IESI 77-fold. The established mechanism is non-competitive with positive cooperativity.

Inhibition of rCPB3 by compound **3c** parabolic replots were observed (**Figures S4B** and S**4C**, Supplementary material). However, the compounds **f12a** and **f12b** (**Figures S5** and S**6,** Supplementary material) demonstrated linear slope and linear intercept replots (**Figures S5B, S5C** and S**6B**, **S6C**, Supplementary material).

The inhibition constants determined for **f12a** were K_i = 7.47 ± 0.64 μM and αK_i = 7.50 ± 0.66 μM. Compound **f12b** presented K_i = 13.7 ± 1.4 μM and αK_i = 13.7 ± 1.2 μM, and both α values were 1, which means that the compounds bind with the same affinity to the free enzyme E or to the ES complex. The **3c** inhibition constants were K_i = 15.4±3.0 μM, αK_i = 141 ± 27 μM, βK_i = 2.21 ± 0.16 μM (β = 0.14) and γK_i = 0.77 ± 0.14 μM(γ = 0.05) (**Table 4**). The α value (α = 9.15) shows that **3c** preferentially binds to the free enzyme. With the binding of the compound to the ES complex that forms ESI defined by the γ factor, the formation of the quaternary IESI complex will be favoured 20-fold. On the other hand, the formation of the EI complex by binding of the first molecule **3c** favours 7-fold the for-

Preprints (www.preprints.org) | NOT PEER-REVIEWED | Posted: 21 November 2022 doi:10.20944/preprints202211.0376.v1

mation of IEI. Therefore, **3c** presented a non-competitive inhibition mechanism with positive cooperativity, while **f12a** and **f12b** presented a simple linear non-competitive inhibition mechanism.

Compounds **3c**, **f12a** and **f12b** showed inhibition profiles of rH84Y as those observed in the inhibition of rCPB3 (**Figures S7**, **S8** and S**9**, Supplementary material). The affinity constants determined for **3c** were K_i = 29.4±4.7 μM, αK_i = 127 ± 20 μM, βK_i = 1.45 ± 0.27 μM and γK_i = 1.06 ± 0.18 μM (**Figures S7E** and S**7F**, Supplementary material). The calculated factors were α = 4.32, β = 0.049 and γ = 0.036 (**Table 4**). Thus, the binding of the first **3c** molecule to the free enzyme favors the formation of IEI 20-fold, and the formation of IESI is favoured 28-fold. The effects of compounds **f12a** and **f12b** showed slope and linear intercept (**Figures S8C**, **S8D**, **S9C** and S**9D**, Supplementary material) replots with values of inhibition constants K_i = 11.2 ± 0.8 μM and αK_i = 11.2 ± 0.5 μM for **f12a**, Ki = 6.08 ± 0.37 μM and αK_i = 6.06 ± 0.24 μM for **f12b**, with α~1 in both cases. Therefore, **3c** presented a non-competitive inhibition mechanism with positive cooperativity and **f12a** and **f12b** presented a simple linear non-competitive inhibition mechanism.

Table 4: Chalcone and flavonoids affinity constants and inhibition mechanisms of enzymes rCPB2.8, rCPB3, and rH84Y.

Compound	Ki (μM)	αKi (μM)	βKi (μM)	γKi (μM)	α	β	γ	Mechanism
rCPB2.8								
3c	100±18	147±28	0,55±0,10	1,15±0,21	1.47	0.0055	0.0115	NCPC
f12a	12,4±1,4	10,7±1,1	3,65±0,39	0,25±0,03	1	0.29	0.02	NCPC
f12b	39,2±4,1	24,9±2,3	1,17±0,12	0,51±0,09	0.634	0.029	0.013	NCPC
rCPB3								
3c	15,4±3.0	141±27	2,21±0,16	0,77±0,14	9.15	0.14	0.05	NCPC
f12a	7,47±0,64	7,50±0,66	---	---	1			SLNC
f12b	13,7±1,4	13,7±1,2	---	---	1			SLNC
rH84Y								
3c	29,4±4,7	127±20	1,45±0,27	1,06±0,18	4.31	0.049	0.036	NCPC
f12a	11,2±0,8	11,2±0,5	---	---	1			SLNC
f12b	6,08±0,37	6,06±0,24	---	---	1			SLNC

NCPC: non-competitive inhibition with positive cooperativity; SLNC: simple linear non-competitive inhibition

2.3. Molecular modeling study

The results of inhibitory capacity and the mechanism of action against these isoforms by the obtained chalcone and flavonol analogs are unprecedented. However, previous work in the literature may shed light to the understanding of the potential binding mode of the compounds at the active site of the CPB isoforms. *L. mexicana* type B cysteine proteases are L-like cathepsins. The inhibition activity of these enzymes by chalcones was already known. Studies by Raghav and Kaur (2015) found that the catalytic CYS 29 thiolate of cathepsin L was able to attack the nucleophilic sites of chalcones [45]. In other recent work, chalcones demonstrated *in vitro* antileishmanial activity on the forms of amastigote and promastigote of *L. infantum*. The suggested mechanism of action was inhibition of pro-cathepsin-L-like by the formation of hydrogen bonds between the amino acid TRP 151 of the active site and the carboxyl group of the chalcones [46]. Isolated flavonoids were also able to inhibit cathepsins L and B in previous studies [47].

Other classes of small molecules have also been described as inhibitors that target multiple cathepsin L-like cysteine proteases, some with overlapping antiparasitic activity [40]. Among them, vinyl sulfones have been shown to be highly potent and selective inhibitors of cathepsins L and B and are also considered antiparasitic prototypes [48,49]. Interestingly, a remarkable 3D similarity was demonstrated by the structural overlap of a crystallographic analogue of vinyl sulfone and the compounds **3c**, **f12b,** and **f12c** and, as a result, a compatible binding mode at the active site of the enzyme (**Figure 4A and 4B,**

 doi:10.20944/preprints202211.0376.v1

respectively). In particular, the overlap with the vinyl sulfone was useful in understanding non-competitive inhibition with a positive cooperativity mechanism. Therefore, the crystal structure of a papain-like cysteine protease bounded with the vinyl sulfone derivative [50] was used as a template in the homology modeling study.

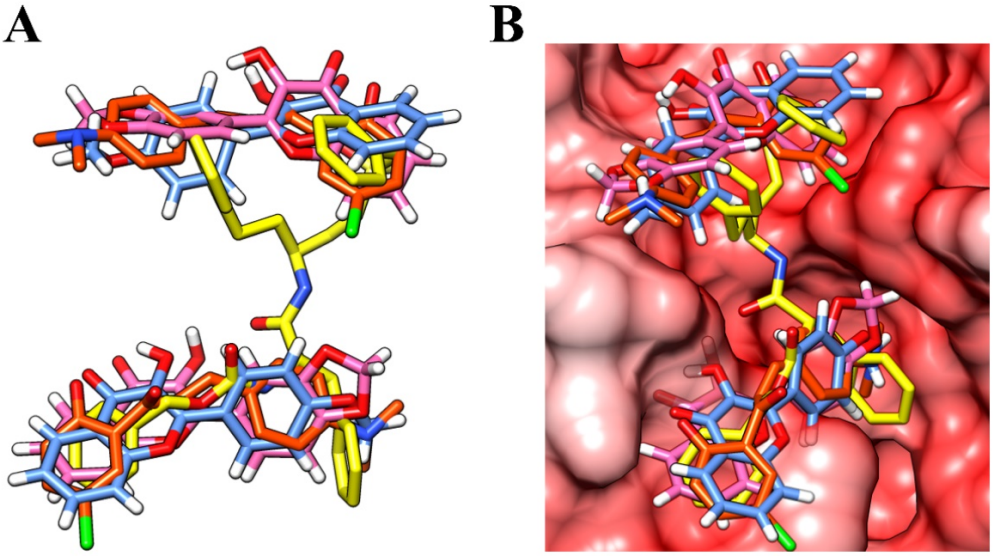

Figure 4: (**A**) Overlay of the vinyl sulfone analog (yellow), compound **3c** (orange), **f12a** (blue) and **f12b** (pink) and the compounds overlayed at the binding site of the enzyme enzyme (**B**).

The isoforms rCPB2.8, rCPB3 and rH84Y have a small number of modifications at their activity sites (**Table S1**, Supplementary material). However, the few amino acid variations between these isoenzymes are important in modifying substrate specificities [43]. This change may have modified either the catalytic or allosteric site, even at a distance. This type of event was observed in substitutions distant from the active site that affect the catalytic activity of CheZ and the binding of CheYp, with possible propagation of structural or dynamic disturbance [51].

Interestingly, even with the amino acid residues variations, chalcone **3c** showed the same mechanism of action on the three isoforms. To investigate its possible binding mode at the active site of the enzymes, the energy values of each pose pointed by 3D overlapping at rCPB2.8 was calculated after the geometry optimization (**Table S2**, Supplementary material). The position with the lower potential energy was also used to investigate the intermolecular interactions at the active site of rCPB3 and rH84Y. Despite to have the same mechanism of action, the calculated binding-free energy values of compound **3c** at the catalytic site of the isoforms was remarkable different (**Table 5**). Particularly, the chalcone had the most promising binding free energy result on rCPB3 (-24.70 kcal mol^{-1}). These values reinforce the hypothesis of a more favorable interactions in a molecular scenario between the compound **3c** and this isoform and corroborates with the *in vitro* results.

On the contrary, the variation of amino acid residues resulted in a different mechanism of action of flavonols **f12a** and **f12b** between the three isoforms. This change is due to the difference in the negative charge distribution of these residues, which necessarily results in significant changes in the electrostatic potential on the surface of the isoenzymes, in addition to providing the parasite with a series of hydrolytic activities [43,52]. Therefore, the change in the electrostatic potential on the surface of the isoenzymes promoted changes in the inhibition mechanisms, as well as differences in the affinity constants.

Following the simple linear non-competitive inhibition mechanism, the potential energy of the different positions of **f12a** at the biding site of rCPB3 were promising (**Table S3**, supplementary material). The binding pose with the lower potential energy was used to investigate the intermolecular interactions of the flavonols analogs at the active site of

 doi:10.20944/preprints202211.0376.v1

rCPB3 and rH84Y, since the mechanism of action was the same at these two isoforms. As well as occurred with compound **3c**, the calculated binding-free energy values of **f12a** at the biding site of the isoforms was notable different, with lowest value for rCPB3 (-5.65 kcal mol^{-1}). This result corroborates with the *in vitro* assays that demonstrate higher affinity constant for this isoform (**Table 5**). Despite the structural similarity, the compound f12b has the lower binding-free energy at the simulations of the active site of rH84Y (**Table 5**). Also, the calculated energy values demonstrated a high difference among the three isoforms (**Table 5**), which corroborates with the considerably lower affinity constant for rCPB2.8.

Table 5: Calculated energy values for the interaction of **3c, f12a and f12b** with the tested rCPB isoforms[a]

Enzyme	Binding-free energy	Δ_E	Ki (μM)
	3c		
rCPB2.8	-2.46	22.24	100±18
rCPB3	-24.70	0	12.4±1.4
rH84Y	-22.49	2.21	39.2±4.1
	f12a		
rCPB2.8	-3.58	2.07	12.4±1,4
rCPB3	-5.65	0	7.47±0,64
rH84Y	-5.24	0.42	11.2±0,8
	f12b		
rCPB2.8	-0.21	5.44	39.2±4,1
rCPB3	-4.30	1.35	13.7±1,4
rH84Y	-5.65	0	6.08±0,37

a: All energy values are expressed in kcal mol^{-1}

Analysing the output results of the simulations of compound **3c**, the variations of amino acid residues at the binding site of the isoforms resulted in a similar occupation of the biding pockets but noticeable differences in the intermolecular interactions (Figures **5A**, **5C** and **5E**). At the binding site of rCPB2.8, **3c** made mainly hydrophobic interactions (**Figure 5B**). However, the substitution of ASP 186 to ASN 186 resulted in the formation of a hydrogen bond, also observed with GLY 144 (**Figure 5D**). This strong intermolecular interaction was conserved at the active site of rH84Y, however the hydrogen bond with GLY 144 was not observed at the catalytic site of this isoform (**Figure 5f**). The difference in intermolecular interactions added to the binding-free energy values corroborates to the affinity constants pointed by *in vitro* assays.

At the active site of rCPB2.8, the molecules of flavonol **f12a** had a great occupation of the biding pockets and made hydrogen bonds with the amino acid residue ASP 189 (**Figures 6A** and **6B**). The number of hydrogen bonds increased at the binding site of rCPB3, since the compound made interactions with TRP 310 and GLY 191 (**Figure 6D**). Previous studies have already discussed the interaction between flavonoid derivatives and GLY amino acid residue of the cathepsin L catalytic site and its importance in stabilizing the active compound at the biding site of the enzyme [45]. The occupation of **f12a** at the binding pockets of rCPB3 and rH84Y was very similar (**Figures 6C** and **6E**). This resemblance was reflected by the interactions with the amino acid residues of the two isoforms (**Figure 6F**).

The binding poses of f12b at rCPB isoforms were very similar to those found for f12a and highly occupies the biding poses of each isoform even by the simple linear non-competitive inhibition mechanism (**Figure 7A**, **7C** and **7E**). At the active site of rH84Y the proximity with the amino acid residue GLY 191 (3.953Å) may be related to a better interaction with this isoform (**Figure 7F**).

Preprints (www.preprints.org) | NOT PEER-REVIEWED | Posted: 21 November 2022 doi:10.20944/preprints202211.0376.v1

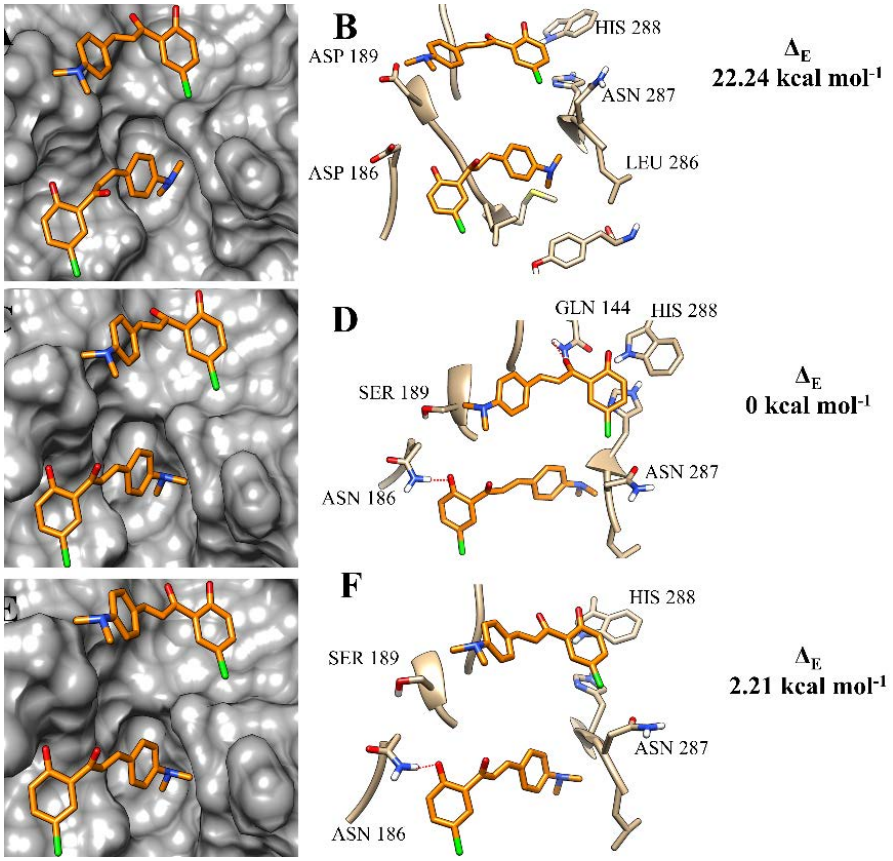

Figure 5: Binding mode positions of chalcone **3c** at the active site of rCPB2.8 (**A**, **B**), rCPB3 (**C**, **D**), and rH84Y (**E**, **F**). The hydrogen bonds are represented by a red dashed line.

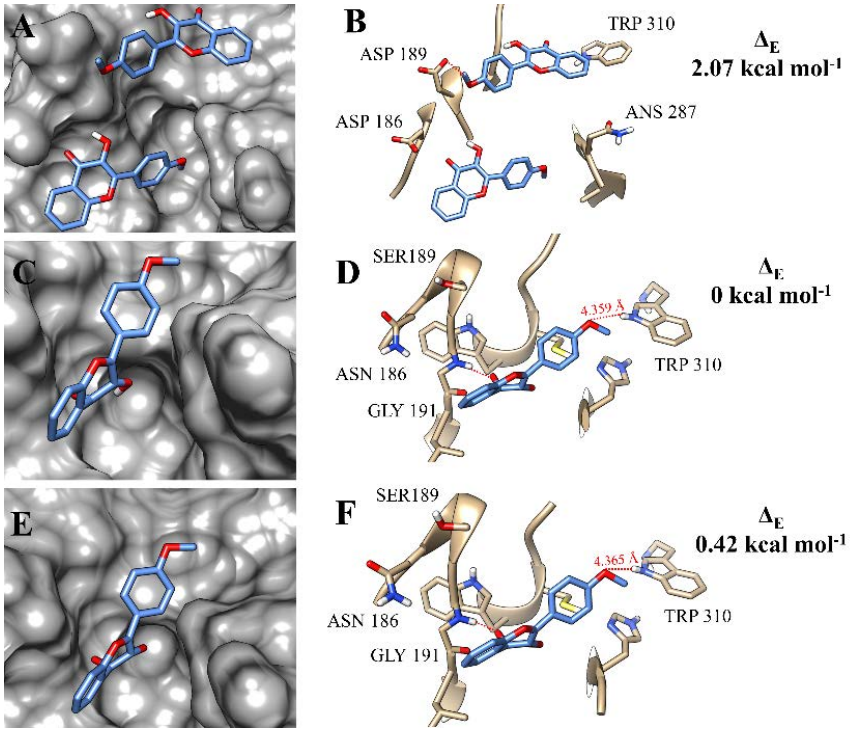

Figure 6: Binding mode positions of flavonol **f12a** at the active site of rCPB2.8 (**A**, **B**), rCPB3 (**C**, **D**), and rH84Y (**E**, **F**). The hydrogen bonds are represented by a red dashed line.

 doi:10.20944/preprints202211.0376.v1

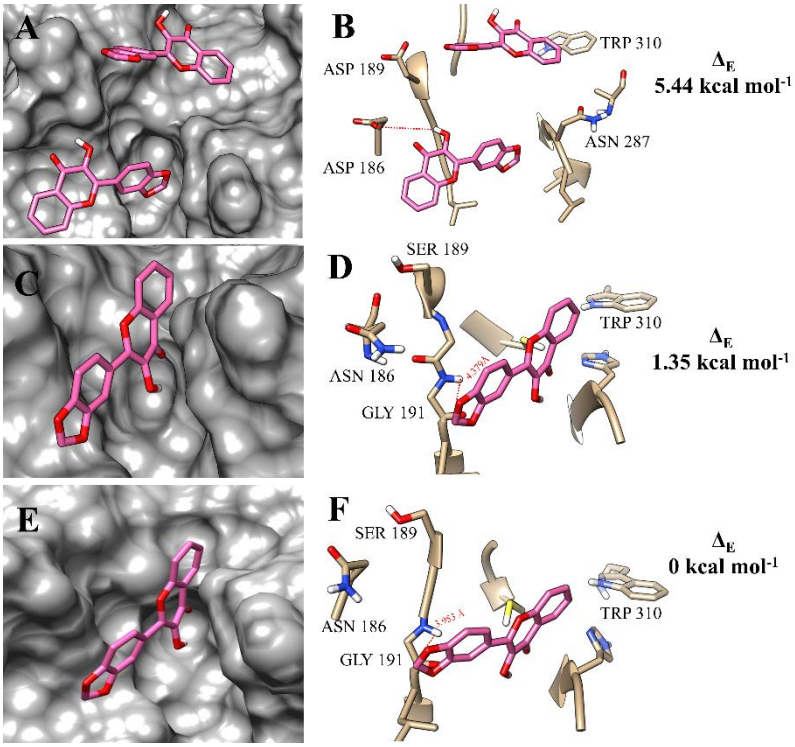

Figure 7: Binding mode positions of flavonol **f12b** at the active site of rCPB2.8 (**A**, **B**), rCPB3 (**C**, **D**), and rH84Y (**E**, **F**). The hydrogen bonds are represented by a red dashed line.

2.4. *Antipromastigote assay and cytotoxicity elucidation*

Although flavonoid derivatives have demonstrated promising enzymatic inhibitory potential, the development of a drug candidate for leishmaniasis treatment depends on several pharmacological aspects. Among them, the cytotoxicity of compounds is crucial for the discovery of a new antileishmanial prototype, since high toxicity still represents a serious limitation of the drugs used in current therapy [53]. The compounds need to be highly active against the *Leishmania* parasite and to provide safety to host cells. This pharmacological characteristic is measured by the selectivity index (SI), defined as the ratio of 50% cytotoxic concentration of mammalian cells (GL_{50}) to half maximum inhibitory concentration on parasites (IC_{50}).

However, the determination of IC_{50} by *in vitro* screening tests is a challenge from the *Leishmania* parasite itself. The *Leishmania* lifecycle requires the presence of a sand fly vector and a mammalian host that causes the existence of two distinct morphological forms (promastigote and amastigote). Although the amastigote form is found in host cells and is considered the target form of the parasite, its determination of IC_{50} consists of a time-consuming and laborious procedure and is not suitable for a large-scale screening method [54]. In general, exploratory screening methods designed to accelerate the testing of many compounds are performed on the promastigote form [54,55]. Therefore, to determine the SI of all flavonoid derivatives, we use he half maximum inhibitory concentration on promastigote forms.

All of the seventeen flavonoid derivatives have in common moderate to low solubility in water. This physical property represents an obstacle in determining the IC_{50} of the compounds, as the test occurs in an aqueous medium. Consequently, the higher concentration tested (10 μg/mL) was lower than that generally described in the literature (50 μg/mL) [56]. Compounds with IC_{50} greater than 10 μg/mL were considered non-active. However, since even the higher concentration tested is lower than that reported for compounds considered active against the parasite, these molecules may not be excluded as potential antileishmanial prototypes.

 doi:10.20944/preprints202211.0376.v1

Among the tested molecules, the chalcone analogs stood out. Compounds **2a**, **3a** and **4c** were more active than the standard drug Pentamidine (IC_{50} = 0.71, 0.60 and 0.50 μM, respectively). Between the derivatives of flavonols, **f12c** has the highest potency against the parasite (IC_{50} = 0.73 μM). The results indicated that the substitution of a chloride atom in the phenolic ring of the chalcone and flavonol derivatives increased the activity against the *Leishmania* promastigote form (**Table 6**).

Compounds **3a** and **4c**, the most active against the promastigote form, were also non-cytotoxic against mammal cells (**Figure S10**, Supplementary material), with an optimal selective index (SI > 1752.48 and 1443.10, respectively) when compared to first-line drugs such as pentamidine and amphotericin B [56] (**Table 6**). It is important to emphasize that all the compounds tested demonstrated low cytotoxicity to mammal cells, resulting in high selective index values.

The lipophilicity (logP) and water solubility (logS) properties of the flavonoid derivatives were also measured by *in silico* analysis. The importance of these chemical characteristics was first discussed by Lipinski et al. (1997) through the publication of the Rule of Fives. In this study, among the physicochemical characteristics of a set of standard drugs, clogP ≤ 5 was postulated as necessary for an ideal prototype [57]. Later, the development of an ADME *in silico* tool, based on the analysis of more than 2000 standard drugs, indicated that more than 80% of the drugs on the market have a (estimated) logS value greater than -4 [58]. All seventeen flavonoid derivatives had logS with values close to -4 and logP ≤ 5, following the postulated by the Rule of Fives. These ADME results added to the biological potential indicate that all synthetic flavonoids are druglike and can be considered promising prototypes for the treatment of leishmaniasis disease.

Table 6: Molecular LogP, LogS, in vitro antileishmanial activity and cytotoxicity of flavonoid analogs.

Entry	Compound	$LogP_{o/w}$[1]	LogS[2]	Promastigote IC_{50} (μM)[3]	NIH/3T3 Cells GL_{50} (μM)[5]	SI[6]
1	**1a**	3.97	-4.59	n.a[4]	294.13	n.d[7]
2	**1b**	3.87	-5.03	n.a[4]	811.27	n.d[7]
3	**1c**	4.04	-4.91	1.14	> 874.83	> 767.39
4	**2a**	3.10	-4.05	0.71	940.14	1324
5	**2b**	2.88	-4.08	n.a[4]	910.58	n.d[7]
6	**2c**	3.17	-4.20	n.a[4]	> 935.21	n.d[7]
7	**3a**	3.64	-4.64	0.60	> 865.86	> 1443.10
8	**3b**	3.46	-4.67	0.96	59.13	61.59
9	**3c**	3.65	-4.79	n.a[4]	> 828.44	n.d[7]
10	**4a**	3.42	-4.20	n.a[4]	901.09	n.d[7]
11	**4b**	3.24	-4.23	1.95	> 873.36	n.d[7]
12	**4c**	3.42	-4.36	0.50	> 876.24	> 1752.48
13	**f12a**	2.83	-4.09	n.a[4]	> 931.93	n.d[7]
14	**f12b**	2.68	-4.11	n.a[4]	> 885.74	n.d[7]
15	**f12c**	2.85	-4.23	0.73	759.13	1039.90
16	**f13a**	3.27	-4.44	1.08	> 825.87	> 764.70
17	**f13c**	3.29	-4.59	n.a[4]	> 791.76	n.d[7]
Doxorubicin		---	---	---	0.05	n.d[7]
Pentamidine		---	---	0.80	---	n.d[7]
Amphotericin B		---	---	0.10	---	n.d[7]

[1]LogP, octanol/water partition coefficient measured by SwissADME [59]; [2]LogS expressed as log (g/100g water measured by SwissADME [59], [3]IC_{50}, half maximum inhibitory concentration on promastigote forms; [4]n.a, not active compound (IC_{50} > 10 μg/mL) [5]GL_{50}, concentration that inhibited cell growth by 50%; [6]SI (selectivity index), IC_{50} in mammalian cells/IC_{50} in extracellular promastigotes; [6]n.d, not determined. The data are representative of three independent experiments.

 doi:10.20944/preprints202211.0376.v1

3. Conclusions

Our synthetic protocols confirmed that they are versatile, scalable, easy to reproduce, and inexpensive methods for obtaining high yields of flavonoid derivatives. The compounds demonstrated the multitarget properties intended by our study to inhibit all tested rCPB isoforms of *L. mexicana*. Between the flavonoid analogs, compounds **3c**, **f12a,** and **f12b** stood out for being effective against all isoforms simultaneously. Interestingly, the *in vitro* study of the mechanism of cysteine protease inhibition showed that the small variations of amino acid residues between the rCPB isoforms were able to change the mechanism of action and biding mode position of the compounds. These findings were confirmed by the *in silico* investigation that demonstrated the formation of strong intermolecular interactions between the compounds and the active site of each enzyme. The compounds were highly potent and demonstrated low cytotoxic action against mammalian cells, proving that the tested molecules are extremely selective. In addition, the calculated values of logP and logS proved that the compounds have ADME properties compatible with those observed in standard drugs. These results show important progress in the investigation of the antileishmanial actions of synthetic flavonoid derivatives and reinforce their potential as prototypes for the design of other cysteine protease inhibitors for the treatment of leishmaniasis.

4. Materials and Methods

4.1. Chemistry

All reagents, purchased from Sigma-Aldrich®, were analytical grade and used without further purification. Reactions were monitored by TLC using Merck 60 F254 precoated silica plates, and spot visualization was achieved with UV light (254 – 360 nm), molybdophosphoric acid (10% w/v) and a solution of sulfur vanillin [0.5 g vanillin in 100 mL of sulfuric acid/methanol (40:10)]. All products were purified by recrystallization from ethanol. The solvents used in the reactions and recrystallization were purified and dried according to procedures found in the literature [60]. A mixture of hexane (Hex) and ethyl acetate (EtOAc) was used in a 1:2 (v/v) proportion as the mobile phase to measure the retention factor (R_f) values of all purified compounds. All melting points were determined using a Quimis® of Brazil model Q340S instrument. The ^{1}H and ^{13}C NMR spectra were recorded on a Bruker Avance DPX-300 or Bruker Ascend 500 spectrometer. Chemical shifts are reported as δ values (ppm) referenced to the residual solvent ($CDCl_3$ at δ 7.24 ppm, DMSO-d_6 at δ 2.50 ppm). Peak multiplicities are abbreviated as follows: singlet; d (doublet); dd (doublet of doublets), tp (triplet of doublets); t (triplet); dt (doublet of triplets); m (multiplet). The coupling constants (*J*) are quoted in Hertz and recorded at the nearest 0.1 Hz.

*4.2. General procedure for the synthesis of chalcone-like compounds by the Claisen-Schmidt reaction (**1a – 4c**)*

The synthesis procedure followed the Claisen-Schmidit reaction methodology described in the literature with modifications [33]. An aqueous solution of NaOH (3 M, 1.6 mL) was added to a solution of aromatic ketone (1 mmol) in EtOH. An ethanolic solution of substituted benzaldehyde was added dropwise to the reaction mixture. The mixture was stirred at room temperature for 24h and then cooled. The reaction mixture was acidified with concentrated HCl (37%) to pH = 2 in an ice bath and under vigorous stirring. The precipitate formed was filtered, washed with cold water, and purified by recrystallization from ethanol.

*4.3. General procedure for the synthesis of flavonol-like compounds by the Algar Flynn-Oyamada reaction (**f12a – f13c**)*

 doi:10.20944/preprints202211.0376.v1

In a bottom-flask, an aqueous solution of NaOH (1 M, 2 mL) was added to 1 mmol of chalcone in EtOH (5 mL). The solution was cooled until an ice-cold suspension was formed. An aqueous solution of H_2O_2 (35%, 250 µL) was added to the ice-cold suspension and the mixture was allowed to warm at room temperature and stirred for 1 - 2 hours. Then, distilled water (3 mL) was added. The reaction mixture was acidified with concentrated HCl (37%) to pH = 2 in an ice bath and under vigorous stirring. The precipitate formed was filtered, washed with cold water, and purified by recrystallization from ethanol.

(*E*)-1-(4-chlorophenyl)-3-(4-methoxyphenyl)prop-2-en-1-one (1a): Pale yellow Crystal. Yield 67.11%. Mp 118 - 120 °C. R_f = 0.535. ^{1}H NMR ($CDCl_3$, 300 MHz) δ ppm 7.96 (2H, d, *J* = 8.6, ArH), 7.81 (1H, d, *J* = 15.6 Hz, C=CH), 7.61 (2H, d, *J* = 8.7, ArH), 7.47 (2H, d, *J* = 8.6, ArH), 7.38 (1H, d, *J* = 15.6 Hz, C=CH), 6.95 (2H, d, *J* = 8.7, ArH), 3.85 (3H, s, -OCH_3); ^{13}C NMR ($CDCl_3$, 75 MHz) δ ppm 189.29, 161.97, 145.32, 139.05, 136.92, 130.45, 129.94, 128.98, 127.54, 119.27, 114.58, 55.54.

(*E*)-3-(benzo[d][1,3]dioxol-5-yl)-1-(4-chlorophenyl)prop-2-en-1-one (1b): Pale yellow Crystal. Yield 86.19%. Mp 126 - 130 °C. R_f = 0.56. ^{1}H NMR ($CDCl_3$, 300 MHz) δ ppm 7.96 (2H, d, *J* = 8.5, ArH), 7.76 (1H, d, *J* = 15.6 Hz, C=CH), 7.48 (2H, d, *J* = 8.5, ArH), 7.33 (1H, d, *J* = 15.6 Hz, C=CH), 7.15 (1H, d, *J* = 1.6 Hz, ArH), 7.13 (1H, dd, *J* = 8.1, ArH), 6.85 (1H, dd, *J* = 8.1, ArH), 6.03 (2H, s, -OCH_2O); ^{13}C NMR ($CDCl_3$, 75 MHz) δ ppm 188.69, 149.80, 148.16, 144.88, 138.74, 136.38, 129.52, 128.87, 125.13, 119.16, 108.41, 106.35, 101.40.

(*E*)-1-(4-chlorophenyl)-3-(4-(dimethylamino)phenyl)prop-2-en-1-one (1c): Yellow amorphous powder. Yield 73.26%. Mp 138 – 140 °C. R_f = 0.40. ^{1}H NMR ($CDCl_3$, 300 MHz) δ ppm 7.96 (2H, d, *J* = 8.6, ArH), 7.82 (1H, d, *J* =15,5 Hz, C=CH), 7.55 (2H, d, *J* = 8.9, ArH), 7.46 (2H, d, *J* = 8.6, ArH), 7.30 (1H, d, *J* =15,5 Hz, C=CH), 6.70 (2H, d, *J* = 8.9, ArH), 3,04 (6H, s, -$N(CH_3)_2$); ^{13}C NMR ($CDCl_3$, 75 MHz) δ ppm 189.94, 151.86, 146.08, 138.12, 137.10, 130.25, 129.43, 128.42, 122.13, 115.90, 111.50, 39.81.

(*E*)-1-(2-hydroxyphenyl)-3-(4-methoxyphenyl)prop-2-en-1-one (2a): Yellow amorphous powder. Yield 76.53%. Mp 90 – 94 °C. R_f = 0.60. ^{1}H NMR ($CDCl_3$, 300 MHz) δ ppm 12.96 (1H, s, OH), 7.92 (1H, dd, *J* = 2.3, 8.6 Hz, ArH), 7.91(1H, d, *J* =15.5 Hz, C=CH), 7.62 (2H, d, *J* = 8.6 Hz, ArH), 7.55 (1H, d, *J* =15.5 Hz, C=CH), 7.50-7.45 (1H, m, ArH), 7.02 (1H, d, *J* = 8.4 Hz, ArH), 6.95 (2H, d, *J* = 8.4 Hz, ArH), 7.00-6.90 (1H, m, ArH), 3,86 (3H, s, -OCH_3); ^{13}C NMR ($CDCl_3$, 75 MHz) δ ppm 193.35, 163.23, 161.72, 145.04, 135.82, 130.24, 129.22, 127.02, 119.80, 118.44, 118.25, 117.25, 114.20, 55.12.

(*E*)-3-(benzo[d][1,3]dioxol-5-yl)-1-(2-hydroxyphenyl)prop-2-en-1-one (2b): Yellow amorphous powder. Yield 71.43%. Mp 138 – 140 °C. R_f = 0.64. ^{1}H NMR ($CDCl_3$, 300 MHz) δ ppm 12.89 (1H, s, OH), 7.90 (1H, 1.7, 8.1 Hz, ArH), 7.86 (1H, d, *J* = 15.5 Hz, ArH), 7.50 (1H, ddd, *J* = 1.7, 7.9, 8.1 Hz, ArH), 7.50 (1H, d, *J* = 15.5 Hz, ArH), 7.17 (1H, d, *J* = 1.7 Hz, ArH), 7.15 (1H, dd, *J* = 1.7, 8.1 Hz, ArH), 7.03 (1H, d, *J* = 8.1 Hz, ArH), 6.92 (1H, t, *J* = 7.2, 7.5, Hz, ArH), 6.86 (1H, d, *J* = 7.9 Hz, ArH), 6.03 (2H, s, -OCH_2O); ^{13}C NMR ($CDCl_3$, 75 MHz) δ ppm 193.23, 163.25, 150.0, 148.20, 145.02, 135.91, 129.21, 128.77, 125.44, 119.76, 118.48, 118.29, 117.69, 108.44, 106.44, 101.45.

(*E*)-3-(4-(dimethylamino)phenyl)-1-(2-hydroxyphenyl)prop-2-en-1-one (2c): Purple crystals. Yield 82.34%. Mp 178 – 181 °C. R_f = 0.71.^{1}H NMR ($CDCl_3$, 300 MHz) δ ppm 13.23 (1H, s, OH), 7.93 (1H, d, *J* = 15.4, C=CH), 7.90 (1H, d, *J* = 5.2 Hz, ArH), 7.57 (2H, d, *J* = 8.9 Hz, ArH), 7.48 (1H, d, *J* = 5.2 Hz, ArH), 7.46 (1H, d, *J* = 15.4, C=CH), 7.01 (1H, d, *J* = 7.9 Hz, ArH), 6.94 (1H, t, *J* = 7.7 Hz, ArH), 6.69 (2H, d, *J* = 8.9 Hz, ArH), 3.04 (6H, s, - $N(CH_3)_2$); ^{13}C NMR ($CDCl_3$, 75 MHz) δ ppm 193.18, 163.16, 152.02, 146.25, 135.32, 130.55, 129.06, 121.97, 120.08, 118.26, 118.13, 113.90, 111.48, 39.76.

(*E*)-1-(5-chloro-2-hydroxyphenyl)-3-(4-methoxyphenyl)prop-2-en-1-one (3a): Yellow amorphous powder. Yield 90.40%. Mp 108 – 109°C. R_f = 0.79. ^{1}H NMR ($CDCl_3$, 500 MHz) δ ppm 12.87 (1H, s, OH), 7.93 (1H, d, *J* = 15.5, C=CH), 7.85 (1H, s, ArH), 7.65 (2H, d, *J* = 8.1 Hz, ArH), 7.45-7.41 (2H, d, *J* = 15.5, C=CH, ArH), 6.98 (3H, m, ArH), 3.87 (3H, s, -OCH_3);

 doi:10.20944/preprints202211.0376.v1

^{13}C NMR ($CDCl_3$, 125 MHz) δ ppm 192.53, 162.17, 161.87, 146.30, 135.77, 130.69, 128.57, 126.92, 123.27, 120.57, 120.03, 116.66, 114.45, 55.35.

(*E*)-3-(benzo[d][1,3]dioxol-5-yl)-1-(5-chloro-2-hydroxyphenyl)prop-2-en-1-one (3b): Yellow amorphous powder. Yield 86.70%. Mp 142 – 146. R_f = 0.72. ^{1}H NMR ($CDCl_3$, 500 MHz) δ ppm 12.80 (1H, s, OH), 7.87 (1H, d, *J* = 15.3 Hz, C=CH), 7.83 (1H, d, *J* = 2.5 Hz, ArH), 7.43 (1H, d, *J* = 8.9, 2.5 Hz, ArH), 7.39 (1H, d, *J* = 15.3 Hz, C=CH), 7.19 (1H, d, *J* = 1.7 Hz, ArH), 6.98 (1H, d, *J* = 8.9 Hz, ArH), 6.87 (1H, *J* = 8.1 Hz, ArH), 6.05 (2H, s, -OCH_2O); ^{13}C NMR ($CDCl_3$, 125 MHz) δ ppm 192.43, 161.88, 150.50, 148.44, 146.27, 135.86, 128.65, 128.54, 126.02, 123.33, 120.52, 120.06, 117.08, 108.67, 106.71, 101.72.

(*E*)-1-(5-chloro-2-hydroxyphenyl)-3-(4-(dimethylamino)phenyl)prop-2-en-1-one (3c): Purple crystals. Yield 81.74%. Mp 161 – 163 °C. R_f = 0.68. ^{1}H NMR ($CDCl_3$, 300 MHz) δ ppm 13.16 (1H, s, OH), 7.95 (1H, d, *J* = 15.1 Hz, C=CH), 7.85 (1H, d, *J* = 2.1 Hz, ArH), 7.58 (2H, d, *J* = 8.7 Hz, ArH), 7.41 (1H, dd, *J* = 8.8, 2.2 Hz, ArH), 7.35 (1H, d, *J* = 15.1 Hz, C=CH), 6.98 (1H, d, *J* = 8.8 Hz, ArH), 6.70 (2H, d, *J* = 8.7 Hz, ArH), 3.06 (6H, s, -OCH_3); ^{13}C NMR ($CDCl_3$, 75 MHz) δ ppm 192.05, 161.65, 152.25, 147.29, 135.00, 130.87, 128.75, 122.86, 121.75, 120.76, 119.70, 113.08, 111.48, 39.76.

(*E*)-1-(5-fluoro-2-hydroxyphenyl)-3-(4-methoxyphenyl)prop-2-en-1-one (4a): Yellow amorphous powder. Yield 84.32%. Mp 124 - 125 °C. R_f = 0.68. ^{1}H NMR ($CDCl_3$, 300 MHz) δ ppm 12.63 (1H, s, OH), 7.95 (1H, d, *J* = 15.3 Hz, C=CH), 7.65 (2H, *J* = 8.7 Hz, ArH), 7.60 (1H, dd, *J* = 9.2, 3.0 Hz, ArH), 7.44 (1H, d, *J* = 15.3 Hz, C=CH), 7.25 (1H, m, ArH), 7.00 (3H, m, ArH), 3.87 (3H, s, -OCH_3); ^{13}C NMR ($CDCl_3$, 75 MHz) δ ppm 192.46 (d, *J* = 2.7 Hz, ArH), 161.98, 159.38 (d, *J* = 1.0 Hz, ArH), 156.12 (d, *J* = 238.7 Hz, ArH), 145.94, 129.48, 126.80, 123.44 (d, (d, *J* = 23.6 Hz, ArH), 119.51 (d, *J* = 7.3 Hz, ArH), 119.4 (d, *J* = 6.3 Hz, ArH), 116.67, 114.28, 113.99, 56.17.

(*E*)-3-(benzo[d][1,3]dioxol-5-yl)-1-(5-fluoro-2-hydroxyphenyl)prop-2-en-1-one (4b): Yellow amorphous powder. Yield 76.51%. Mp 168 – 171 °C. R_f = 0.72. ^{1}H NMR ($CDCl_3$, 300 MHz) δ ppm 12.61 (1H, s, OH), 7.89 (1H, d, *J* = 15.3 Hz, C=CH), 7.58 (1H, dd, *J* = 9.2, 2.8 Hz, ArH), 7.38 (1H, d, *J* = 15.3 Hz, C=CH), 7.27 (1H, m, 1H), 7.21-7.15 (2H, m, ArH), 7.01 (1H, dd, *J* = 9.1, 4.6 Hz, ArH), 6.88 (1H, d, *J* = 7.9 Hz, ArH), 6.05 (2H, s, -OCH_2O); ^{13}C NMR ($CDCl_3$, 75 MHz) δ ppm 192.38 (d, *J* = 2.7 Hz, ArH), 159.40 (d, *J* = 1.1 Hz, ArH), 156.12 (d, J = 238.2 Hz), 150.28, 148.29, 145.94, 128.54, 125.75, 123.57 (d, J = 23.4 Hz), 119.56 (d, J = 7.3 Hz), 117.10, 114.29 (d, J = 23.4 Hz), 108.51, 106.51, 101.55.

(*E*)-3-(4-(dimethylamino)phenyl)-1-(5-fluoro-2-hydroxyphenyl)prop-2-en-1-one (4c): Red crystals. Yield 95.69%. Mp 186 – 189 °C. R_f = 0.48. ^{1}H NMR ($CDCl_3$, 300 MHz) δ ppm 12.96 (1H, s, OH), 7.94 (1H, d, *J* = 15.1 Hz, C=CH), 7.56 (3H, d, *J* = 8.7 Hz, ArH), 7.31 (1H, d, *J* = 15.1 Hz, C=CH), 7.22-7.15 (1H, m, ArH), 6.98 (1H, dd, *J* = 4.5, 9.1 Hz, ArH), 6.69 (2H, d, *J* = 8.5 Hz, ArH), 3.04 (6H, s, -OCH_3); ^{13}C NMR ($CDCl_3$, 75 MHz) δ ppm 192.10 (d, *J* = 2.8 Hz), 159.26, 156.04 (d, *J* = 237.0 Hz), 152.18, 147.11, 130.77, 122.77 (d, *J* = 23.7 Hz), 121.70, 119.65 (d, *J* = 6.1 Hz), 119.27 (d, *J* = 7.7 Hz), 114.15 (d, *J* = 23.3 Hz), 113.15, 111.46, 39.74.

3-hydroxy-2-(4-methoxyphenyl)-4H-chromen-4-one (f12a): Yellow amorphous powder. Yield 71.34%. Mp 233 – 235 °C. R_f = 0.39. ^{1}H NMR (DMSO-d_6, 500 MHz) δ ppm 9.24 (1H, s, OH), 8.20 (2H, dt, *J* = 8.9, 3.0, 2.1 Hz, ArH), 8.12 (1H, dd, *J* = 6.3, 1.5 Hz, ArH), 7.77 (1H, dt, *J* = 7.8, 1.0 Hz, ArH), 7.72 (1H, dd, J = 8.6, 1.0 Hz, ArH), 7.45 (1H, dt, *J* = 7.8, 1.0 Hz, ArH), 7.12 (2H, dt, *J* = 8.9, 3.0, 2.1 Hz, ArH), 3.85 (3H, s, -OCH_3); ^{13}C NMR (DMSO-d_6, 125 MHz)) δ ppm 172.48, 160.37, 154.35, 145.52, 137.95, 133.25, 129.24, 124.57, 124.26, 123.48, 121.23, 118.09, 113.91, 55.21.

2-(benzo[d][1,3]dioxol-5-yl)-3-hydroxy-4H-chromen-4-one (f12b): Yellow amorphous powder. Yield 69.87%. Mp 213 – 215 °C. R_f = 0.39. ^{1}H NMR (DMSO-d_6, 300 MHz) δ ppm 9.52 (1H, s, OH), 8.10 (1H, d, *J* = 8.1 Hz, ArH), 7.84 (1H, dd, *J* = 8.5, 1.6 Hz, ArH), 7.78-7.73 (3H, m, ArH), 7.47 (1H, td, *J* = 8.1, 6.4, 1.7 Hz, ArH), 7.11 (1H, d, *J* = 8.3 Hz, ArH), 6.12 (2H, s, -OCH_2O); ^{13}C NMR (DMSO-d_6, 75 MHz) δ ppm 172.68, 154.40, 148.54, 147.52, 145.10, 138.33, 133.54, 125.05, 124.69, 122.76, 121.25, 118.36, 108.43, 107.52, 101.67.

2-(4-(dimethylamino)phenyl)-3-hydroxy-4H-chromen-4-one (f12c): Orange crystals. Yield 79.40%. Mp 182 – 183 °C. R_f = 0.39. ^{1}H NMR (DMSO-d_6, 500 MHz) δ ppm 9.16 (1H, s,

 doi:10.20944/preprints202211.0376.v1

OH), 8.12 (1H, d, *J* = 8.8 Hz, ArH), 8.09 (1H, dd, *J* = 7.8, 1.4 Hz, ArH), 7.69-7.75 (2H, m, ArH), 7.44 (1H, t, *J* = 7.3, 7.4 Hz, ArH), 6.83 (2H, d, *J* = 8.8 Hz, ArH), 2.99 (6H, s, -N(CH_3)$_2$); ^{13}C NMR (DMSO-*d*$_6$, 125 MHz) δ ppm 171.98, 154.29, 151.03, 146.85, 137.29, 133.09, 128.99, 124.65, 124.32, 121.45, 118.15, 117.93, 111.40, 39.64.

6-chloro-3-hydroxy-2-(4-methoxyphenyl)-4H-chromen-4-one (f13a): Yellow amorphous powder. Yield 86.42%. Mp 207 – 208 °C. R$_f$ = 0.52. ^{1}H NMR (DMSO-*d*$_6$, 500 MHz) δ ppm 9.44 (1H, s, OH), 8.19 (2H, dt, *J* = 9.2, 2.9 Hz, ArH), 8.02 (1H, t, *J* = 1.4 Hz, ArH), 7.79 (2H, d, *J* = 1.8 Hz, ArH), 7.12 (2H, dt, *J* = 9.2, 2.9 Hz, ArH), 3.85 (3H, s, -OCH_3); ^{13}C NMR (DMSO-*d*$_6$, 125 MHz) δ ppm 171.42, 160.54, 152.86, 146.13, 138.12, 133.11, 129.37, 128.78, 123.18, 122.39, 120.64, 113.94, 55.25.

6-chloro-2-(4-(dimethylamino)phenyl)-3-hydroxy-4H-chromen-4-one (f13c): Orange crystals. Yield 78.67%. Mp 235 – 238 °C. R$_f$ = 0.57. ^{1}H NMR (DMSO-*d*$_6$, 500 MHz) δ ppm 8.98 (1H, s, OH), 8.11 (2H, dt, *J* = 9.1, 3.0 Hz, ArH) 7.99 (1H, t, *J* = 1.7 Hz, ArH), 7.73-7.71 (2H, m, ArH), 6.83 (2H, dt, *J* = 9.1, 3.0 Hz, ArH), 7.11 (1H, d, *J* = 8.3 Hz, ArH), 3.01 (6H, s, -N(CH_3)$_2$); ^{13}C NMR (DMSO-*d*$_6$, 125 MHz) δ ppm 170.51, 152.57, 151.01, 147.28, 137.03, 132.45, 128.75, 128.44, 123.14, 122.36, 120.20, 117.40, 111.12, 39.25.

4.4. Screening the inhibitory activity of compounds

The screening assays for the inhibitory activity of the compounds in the enzymes rCPB2.8, rCPB3, and rH84Y, were performed using 100 mM sodium acetate buffer containing 5 mM EDTA, 100 mM NaCl, 0.01% Triton X-100, 20 % glycerol, at pH 5.5. Enzyme aliquots were pre-incubated with 5 mM DTT for 5 minutes at 37 ° C. After checking the initial rate of the reaction corresponding to the control, the enzymatic rate was measured at two concentrations of compounds, 1 µM and 5 µM. Enzyme activity was monitored by hydrolysis of the substrate Z-FR-MCA by measuring fluorescence at λex = 360 nm and λem = 480 nm on a Hitachi F2700 spectrofluorometer, obtaining the rate values in UAF/min (Arbitrary fluorescence units by minute).

4.5. Determination of IC50 values for inhibitors

Cysteine proteases rCPB2.8, rCPB3, and rH84Y were assayed in 100 mM sodium acetate buffer containing 5 mM EDTA, 100 mM NaCl, 0.01% Triton X-100, 20 % glycerol, at pH 5.5. The enzymes were pre-incubated in the presence of 5 mM DTT for 5 min at 37°C in a 1 mL final volume with constant stirring. Enzyme activities were monitored using fluorogenic probe Z-FR-AMC (9.25 µM final concentration), and the fluorescence was monitored by spectrofluorometry using fluorometer F2700 (Hitachi, Tokyo, Japan) set to λ_{Ex} = 360 nm and λ_{Em} = 480 nm. The inhibitory potential (IC_{50}) was performed in a progressive increase *in the* concentration *of the* compounds and the IC_{50} values were calculated using nonlinear regression and the data were analyzed by Grafit 5.0.13 software using Equation 1

$$y = \frac{100\%}{1 + \left(\frac{x}{IC_{50}}\right)^S} \qquad \text{Eq.1}$$

4.6. Enzyme kinetics and determination of the mechanism of inhibition

Studies of cysteine proteases rCPB2.8, rCPB3 and rH84Y inhibition kinetics were performed in different concentrations of Z-FR-AMC in the presence and absence of compounds using 100 mM sodium acetate buffer containing 5 mM EDTA, 100 mM NaCl, 0.01% Triton X-100, 20 % glycerol, at pH 5.5. Aliquots of the enzymes were pre-incubated with 5 mM DTT for 5 minutes at 37°C. For every kinetic measurement, the compounds were pre-incubated with each enzyme for 10 minutes before adding the substrate. All kinetic assays were performed in duplicate. Inhibition constants were determined using different equations, depending on the inhibition mechanism. The assumed K_M values of

Preprints (www.preprints.org) | NOT PEER-REVIEWED | Posted: 21 November 2022 doi:10.20944/preprints202211.0376.v1

rCPB2.8, rCPB3 and rH84Y for Z-FR-AMC were 3.23 μM, 2.99 μM and 2.80 μM, respectively. The data of the activity rate and substrate concentration generated rectangular hyperbolic profiles that were linearized using the Lineweaver Burk/double reciprocal plot. The replot profiles of the slope vs inhibitor and intercept vs inhibitor provided Ki and αKi parameters, respectively. If the replots present a parabolic profile, there will be in this system the participation of a second molecule of the compound that can bind the enzyme complexed to the first compound (EI) forming IEI and bind to the ESI complex forming IESI. Linearization will be required generating the $1/K_{slope}$ vs inhibitor and $1/K_{intercept}$ vs inhibitor replots according to the Equations 2 and 3.

$$\frac{1}{K_{slope}} = \frac{1}{K_i} + \frac{[I]}{\beta K_i^2} \quad \text{Eq.2}$$

$$\frac{1}{K_{intercept}} = \frac{1}{\alpha K_i} + \frac{[I]}{\alpha\gamma K_i^2} \quad \text{Eq.3}$$

where Ki is inhibitory constant, [I] is the concentration of inhibitor, α is the factor of formation of complex ESI (enzyme-substrate-inhibitor complex), β is the factor of formation of IEI (inhibitor-enzyme-inhibitor) and γ is the factor of formation of IESI (inhibitor, enzyme-substrate-inhibitor) according to the general mechanism (**Figure 8**). Furthermore, β and γ measure the cooperativity between the binding of the first and second inhibitor molecules to form IEI and IESI, respectively.

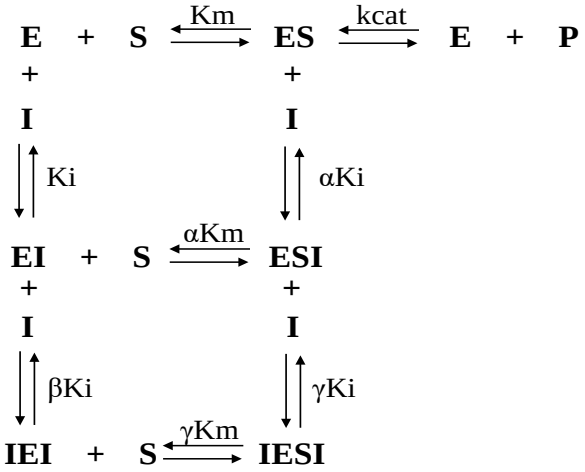

Figure 8: General mechanism of inhibition of cooperativity involving binding of a compound to the free enzyme E and the ES complex

4.7. Molecular modeling

Compounds **3c**, **f12a**, and **f12b** had their 3D structure drawn using the program MarvinSketch 16.9.5 (ChemAxon Ltd.). The optimization was carried out using the PM7 semi empirical method incorporated in the software MOPAC2016[61]. A pH of 7.4 was considered for the definition of charges.

The three-dimensional structure of rCPB2.8 was obtained through the homology modeling methodology using the Swiss-Model program [62]. Therefore, as a layout we used the 3D structure of papain-like cysteine protease obtained from the Protein Data Bank (PDB ID: 1F2A)[50] and the primary structure of rCPB2.8 was the target Sequence. The choice of the crystal was made based on the similarity with the rCPB2.8 and between the tested compound and crystallographic ligand. To determine the potential binding modes at the active site of rCPB2.8, different binding poses were obtained based on the overlay between the tested molecules and the crystallographic ligand. For the compounds with non-competitive inhibition with a positive cooperativity mechanism, we manually added a second molecule in different positions. The 3D structures of rCPB3 and rH84Y

 doi:10.20944/preprints202211.0376.v1

were obtained based on the differences in amino acid residues at their active sites described in the literature using the program UCSF Chimera [63]. All the biding poses were further geometry optimized.

Geometry optimizations were made using the GROMACS 2018 package [64] and the CHARMM force field [65]. The ligand topology was obtained from Swiss Param Server [66] and the properties of the solvent were mimetic based on the TIP3P water model. A cubic box was used to guarantee a space of 1.2 nm between the protein and the box walls, and ions under physiological conditions (0.15 μM) in order to neutralize the system charges. The energy optimization steps were performed using the steepest descent followed by the conjugated gradient algorithm. The convergent criterion was a maximum force of 50 N on the atoms. The potential binding energy was measured, and the position of the binding mode with the best result was used to analyze the interactions with the binding site of all isoforms.

4.8. Citotoxicity on mammalian cells

The cytotoxic effect of the test samples was evaluated on NIH/3T3 fibroblasts, obtained from the Rio de Janeiro Cell Bank (Brazil). Cells were seeded in 96- well plates ($5x10^{e5}$ cells/well). After 24 hours of fixation, cells were incubated for 48 hours with test samples at 0.25-250 μg/mL. in triplicate. The compounds tested were dissolved in DMSO (Sigma-Aldrich® SP/Brazil) while ensuring that the final concentration of the latter (0.25% at the highest sample concentration) did not interfere with cell viability. Doxorubicin (0.025–25 μg/mL, DXR) was used as a positive control. Cells were fixed by adding 20% trichloroacetic acid and subsequently stained with sulforhodamine B (SRB; 0.1%) diluted in acetic acid after 48h of exposure [67]. Absorbance values were read on the PT-READER microplate instrument (Thermoplate®) and growth percentages were calculated according to procedures in the literature [68]. Cytotoxicity activity was expressed as the concentration of drugs that inhibited cell growth by 50% (GL_{50}) and growth was determined by non-linear regression using Origin 6.0 software (OriginLab). The statistical significance was analyzed using an unpaired Student's t-test or a one-way analysis of variance. $P < .05$ was considered statistically relevant. In addition, the selectivity index (SI) was calculated using the ratio between cytotoxicity in NHI-3T3 cells (GL_{50}) and activity in the parasite forms (IC_{50}).

4.9. Parasites

A standard strain of *Leishmania (Leishmania) amazonensis* (IFLA/BR/1967/PH8) was used for the evaluation of *in vitro* antileishmanial activity. The promastigote forms were grown in Schneider's insect medium (Sigma-Aldrich®, SP/Brazil) supplemented with 20% fetal bovine serum (Sigma-Aldrich®, SP/Brazil), 10.000 U/mL penicillin and 10 mg/mL streptomycin (Sigma-Aldrich®, SP/Brazil). Skin lesions were routinely isolated from previously induced skin lesions in BALB/c mice and kept in axenic culture until the 20th serial passage.

4.10. Antipromastigote assay

Promastigote forms of *L. amazonensis* in the log growth phase (10^{e6} parasites/mL) were added to 96-well plates and incubated in sextuplicate with the test samples (0.25 - 10.0 μg/ml). The microplates were incubated at 26 °C for 72 hours. Cell viability was assessed by adding 5 mg/mL of MTT ([3-(4,5-dimethylthiazol-2-yl)-2,5-diphenyltetrazolium bromide] (Sigma-Aldrich® SP/Brazil; 5mg/mL).20 Results were expressed as the half-maximal inhibitory concentration (IC_{50}) calculated by a nonlinear dose-response regression curve using the statistical program GraphPad PRISM 5.0. Pentamidine (Sigma-Aldrich ® SP/Brazil; 0.25 - 10 μg/mL) was used as a positive control and pure Schneider culture medium as a negative control.

Supplementary Materials: The supplementary material comprises the results of the enzyme kinetics and determination of the mechanism of inhibition in vitro tests. Also, we present the NMR spectra section of all synthetic compounds. The following supporting information can be downloaded at: www.mdpi.com/xxx/s1, Figure S1-S10; Table S1-S3, Spectra 1-34.

Author Contributions: EMGL, CCPA, WASJ, RTP, EGB, and DPL conceived and designed the experimental tests. The development of the methodology was made by EMGL, JFL, FS, MMM, and DPL. Analyzes of the data was made by EMGL, CCPA, WASJ, RTP, EGB and DPL. Contributed reagents/Materials/Analysis: RTP, CCPA, FLBF, JPO, AB, and JR. The manuscript was written and reviewed by EMGL, CCPA, WASJ, JR, and DPL. All authors have read and agreed to the published version of the manuscript.

Funding: This study was supported by the Coordenação de Aperfeiçoamento de Pessoal de Nível Superior - Brazil (CAPES) - Finance Code 001, and Fundação de Amparo e Pesquisa do Estado de São Paulo-FAPESP grants nº 2014/02205-1, 2016/25112-4, and 2021/01503-2 (WASJ). JR is grateful to Conselho Nacional de Desenvolvimento Científico e Tecnológico - Brazil (CNPq) for funding (315399/2020-1; and 422645/2021-4)

Data Availability Statement: All datasets generated for this study are included in the article/Supplementary Material.

Acknowledgments: The authors acknowledge Conselho Nacional de Desenvolvimento Científico e Tecnológico - Brazil (CNPq), PROPP-UFMS, Fundação de Apoio ao Desenvolvimento do Ensino, Ciência e Tecnologia – Brazil (FUNDECT – MS), to High-Performance Computing Center at UFRN (NPAD/UFRN) and Fundação de Amparo ao Ensino e Pesquisa da Universidade de Mogi das Cruzes (FAEP/UMC) for the support offered in this research.

Conflicts of Interest: The authors declare that the research was conducted in the absence of commercial or financial relationships that could be construed as a potential conflict of interest.

References

1. BRASIL Doenças Tropicais Negligenciadas; 2021.
2. Brindha, J.; Balamurali, M.M.; Chanda, K. An Overview on the Therapeutics of Neglected Infectious Diseases—Leishmaniasis and Chagas Diseases. *Front Chem* **2021**, *9*, 622286.
3. Alvar, J.; Yactayo, S.; Bern, C. Leishmaniasis and Poverty. *Trends Parasitol* **2006**, 22, 552-557.
4. Fitzpatrick, C.; Engels, D. Leaving No One behind: A Neglected Tropical Disease Indicator and Tracers for the Sustainable Development Goals. *Int Health* **2015**, *8*, i15-8.
5. Ramsay, R.R.; Popovic-Nikolic, M.R.; Nikolic, K.; Uliassi, E.; Bolognesi, M.L. A Perspective on Multi-Target Drug Discovery and Design for Complex Diseases. *Clin Transl Med* **2018**, *7*, 3.
6. Barbosa Gomes de Carvalho, Y.M.; Shanmugam, S.; Batista, M.S.; Serafini, M.R.; Araújo, A.A.D.S.; Quintans Júnior, L.J. Pharmaceutical Agents for Treatment of Leishmaniasis: A Patent Landscape. *Expert Opin Ther Pat* **2020**, *30*, 633-641.
7. Dias, M.C.; Pinto, D.C.G.A.; Silva, A.M.S. Plant Flavonoids: Chemical Characteristics and Biological Activity. *Molecules* **2021**, *26*, 5377.
8. Carter, N.S.; Stamper, B.D.; Elbarbry, F.; Nguyen, V.; Lopez, S.; Kawasaki, Y.; Poormohamadian, R.; Roberts, S.C. Microorganisms Natural Products That Target the Arginase in Leishmania Parasites Hold Therapeutic Promise. *Microorganisms* **2021**, *9*, 267.
9. Gervazoni, L.F.O.; Gonçalves-Ozório, G.; Almeida-Amaral, E.E. 2′-Hydroxyflavanone Activity in Vitro and in Vivo against Wild-Type and Antimony-Resistant Leishmania Amazonensis. *PLoS Negl Trop Dis* **2018**, *12*, e0006930.
10. Braga, F.C.; Ojeda, M.; Perdomo, R.T.; de Albuquerque, S.; Rafique, J.; de Lima, D.P.; Beartriz, A. Synthesis of cardanol-based 1,2,3-triazoles as potential green agents against neoplastic cells. *Sustain Chem Pharm* **2021**, *20*, 100408.
11. Saba, S.; dos Santos, C.R.; Zavarise, B.R.; Naujorks, A.A.S.; Franco, M.S.; Schneider, A.R.; Scheide, M.R.; Affeldt, R.F.; Rafique, J.; Braga, A.L. Photoinduced, Direct C(sp2)–H Bond Azo Coupling of Imidazoheteroarenes and Imidazoanilines with Aryl Diazonium Salts Catalyzed by Eosin Y. *Chem Euro J* **2020**, 26, 4461-4466
12. Galant, L.S.; Rafique, J.; Braga, A.L.; Braga, F.C.; Saba, S.; Radi, R.; da Rocha, J.B.T.; Santi, C.; Monsalve, M.; Farina, M.; de Bem, A.F. The Thiol-Modifier Effects of Organoselenium Compounds and Their Cytoprotective Actions in Neuronal Cells. *Neurochem Res* **2021**, *46*, 120-130.
13. Franco, M.S.; Saba, S.; Rafique, J.; Braga, A.L. KIO_4-mediated Selective Hydroxymethylation/Methylenation of Imidazo-Heteroarenes: A Greener Approach. *Angew Chem* **2021**, *1333*, 18602-18608; *Angew Chem Int Ed Engl* **2021**, *60*, 18454-18460.
14. Veloso, I.C.; Delanogare, E.; Machado, A.E.; Braga, S.P.; Rosa, G.K.; de Bem, A.F.; Rafique, J.; Saba, S.; da Trindade, R.N.; Galetto, F.Z.; Moreira, E.L.G. A selanylimidazopyridine (3-SePh-IP) reverses the prodepressant- and anxiogenic-like effects of a high-fat/high-fructose diet in mice. *J. Pharm. Pharmacol* **2021**, *73*, 673–681.

15. Peterle, M.M.; Scheide, M.R.; Silva, L.T.; Saba, S.; Rafique, J.; Braga, A.L. Copper-Catalyzed Three-Component Reaction of Oxadiazoles, Elemental Se/S and Aryl Iodides: Synthesis of Chalcogenyl (Se/S)-Oxadiazoles. *ChemsitrySelect* **2018**, *3*, 13191-13196.
16. dos Santos, D.C.; Rafique, J.; Saba, S.; Grinevicuis, V.M.A.S.; Filho, D.W.; Zamoner, A.; Braga, A.L.; Pedrosa, R.C.; Ourique, F. IP-Se-06, a Selenylated Imidazo[1,2-*a*]pyridine, Modulates Intracellular Redox State and Causes Akt/mTOR/HIF-1α and MAPK Signaling Inhibition, Promoting Antiproliferative Effect and Apoptosis in Glioblastoma Cells. *Oxid Med Cell Longev* **2022**, ID 3710449.
17. Frizon, T.E.A.; Cararo, J.H.; Saba, S.; Dal-Pont, G.C.; Michels, M.; Braga, H.C.; Pimentel, T.; Dal-Pizzol, F.; Valvassori, S.S.; Rafique, J. Synthesis of Novel Selenocyanates and Evaluation of Their Effect in Cultured Mouse Neurons Submitted to Oxidative Stress. *Oxid Med Cell Longev* **2020**, ID 5417024.
18. Rahman, A.F.M.M.; Ali, R.; Jahng, Y.; Kadi, A.A. A Facile Solvent Free Claisen-Schmidt Reaction: Synthesis of α,α'-Bis-(Substituted-Benzylidene)Cycloalkanones and α,α'-Bis-(Substituted-Alkylidene)Cycloalkanones. *Molecules* **2012**, 17, 571-583.
19. Wang, P.; Li, H.F.; Zhao, J.Z.; Du, Z.H.; Da, C.S. Organocatalytic Enantioselective Cross-Aldol Reaction of o-Hydroxyarylketones and Trifluoromethyl Ketones. *Org Lett* **2017**, *19*, 2634–2637.
20. Wang, Z. Algar-Flynn-Oyamada (AFO) Reaction. In Comprehensive Organic Name Reactions and Reagents; 2010.
21. Gopinath, V.S.; Pinjari, J.; Dere, R.T.; Verma, A.; Vishwakarma, P.; Shivahare, R.; Moger, M.; Kumar Goud, P.S.; Ramanathan, V.; Bose, P.; Rao, M.V.S.; Gupta, S.; Puri, S.K.; Launay, D.; Martin, D. Design, Synthesis and Biological Evaluation of 2-Substituted Quinolines as Potential Antileishmanial Agents. *Eur J Med Chem* **2013**, *69*, 527-536.
22. Neuenschwander, A.; Rocha, V.P.C.; Bastos, T.M.; Marcourt, L.; Morin, H.; da Rocha, C.Q.; Grimaldi, G.B.; de Sousa, K.A.F.; Borges, J.N.; Rivara-Minten, E.; Wolfender, J.-L.; Soares, M.B.P.; Queiroz, E.F. Production of Highly Active Antiparasitic Compounds from the Controlled Halogenation of the Arrabidaea Brachypoda Crude Plant Extract. *J Nat Prod* **2020**, *83*, 2631-2640.
23. Filarowski, A.; Koll, A.; Kochel, A.; Kalenik, J.; Hansen, P.E. The Intramolecular Hydrogen Bond in Ortho-Hydroxy Acetophenones. *J Mol Struct* **2004**, 700, 67-72.
24. Gomes, M.N.; Muratov, E.N.; Pereira, M.; Peixoto, J.C.; Rosseto, L.P.; Cravo, P.V.L.; Andrade, C.H.; Neves, B.J. Chalcone Derivatives: Promising Starting Points for Drug Design. *Molecules* **2017**, *22*, 1210.
25. Rai, P.; Chettri, P.; Kar, S.; Nagar, M.A.; Srivastava, S.; Golakoti, N.R. Synthesis, Characterization and Structure–Activity Relationship of Non-Linear Optical Response of Chalcone Derivatives with in Silico Insights. *Chem Pap* **2021**, *75*, 2603–2615.
26. Montes-Avila, J.; Díaz-Camacho, S.P.; Sicairos-Félix, J.; Delgado-Vargas, F.; Rivero, I.A. Solution-Phase Parallel Synthesis of Substituted Chalcones and Their Antiparasitary Activity against Giardia Lamblia. *Bioorg Med Chem* **2009**, *17*, 6780-6785..
27. Regenass, P.; Abboud, D.; Daubeuf, F.; Lehalle, C.; Gizzi, P.; Riché, S.; Hachet-Haas, M.; Rohmer, F.; Gasparik, V.; Boeglin, D.; Haiech, J.; Knehans, T.; Rogan, D.; Heissler, D.; Marsol, C.; Villa, P.; Galzi, J.-L.; Hibert, M.; Frossard, N.; Bonnet, D. Discovery of a Locally and Orally Active CXCL12 Neutraligand (LIT-927) with Anti-Inflammatory Effect in a Murine Model of Allergic Airway Hypereosinophilia. *J Med Chem* **2018**, 61, 7671–7686.
28. Detsi, A.; Majdalani, M.; Kontogiorgis, C.A.; Hadjipavlou-Litina, D.; Kefalas, P. Natural and Synthetic 2′-Hydroxy-Chalcones and Aurones: Synthesis, Characterization and Evaluation of the Antioxidant and Soybean Lipoxygenase Inhibitory Activity. *Bioorg Med Chem* **2009**, *17*, 8073-8085.
29. Park, S.; Kim, H.J. Highly Activated Michael Acceptor by an Intramolecular Hydrogen Bond as a Fluorescence Turn-on Probe for Cyanide. *Chem Commun* **2010**, *46*, 9197-9199.
30. Mewett, K.N.; Fernandez, S.P.; Pasricha, A.K.; Pong, A.; Devenish, S.O.; Hibbs, D.E.; Chebib, M.; Johnston, G.A.R.; Hanrahan, J.R. Synthesis and Biological Evaluation of Flavan-3-Ol Derivatives as Positive Modulators of GABAA Receptors. *Bioorg Med Chem* **2009**, *17*, 7156-73.
31. Kamecki, F.; Knez, D.; Carvalho, D.; Marcucci, C.; Rademacher, M.; Higgs, J.; Žakelj, S.; Marcos, A.; de Tezanos Pinto, F.; Abin-Carriquiry, J.A.; Gobec, S.; Colettis, N.; Marder M. Multitarget 2′-Hydroxychalcones as Potential Drugs for the Treatment of Neurodegenerative Disorders and Their Comorbidities. *Neuropharmacology* **2021**, *201*, 108837.
32. Zhao, P.L.; Liu, C.L.; Huang, W.; Wang, Y.Z.; Yang, G.F. Synthesis and Fungicidal Evaluation of Novel Chalcone-Based Strobilurin Analogues. *J Agric Food Chem* **2007**, *55*, 5697–5700.
33. Borsari, C.; Santarem, N.; MacEdo, S.; Jiménez-Antón, M.D.; Torrado, J.J.; Olías-Molero, A.I.; Corral, M.J.; Tait, A.; Ferrari, S.; Costantino, L.; Luciani, R.; Ponterini, G.; Gul, S.; Kuzikov, M.; Ellinger, B.; Behrens, B.; Reinshagen, J.; Alunda, J.M.; Cordeiro-da-Silva, A.; Costi, M.P. SAR Studies and Biological Characterization of a Chromen-4-One Derivative as an Anti- Trypanosoma Brucei Agent. *ACS Med Chem Lett* **2019**, *10*, 528–533.
34. Muller, B.M.; Mai, J.; Yocum, R.A.; Adler, M.J. Impact of Mono- and Disubstitution on the Colorimetric Dynamic Covalent Switching Chalcone/Flavanone Scaffold. *Org Biomol Chem* **2014**, *12*, 5108-5114.
35. Gharpure, M.; Chaudhary, R.G.; Juneja, H.; Ingle, V.; Gandhare, N. Oxovanadium (IV) Complexes of 2-Aryl/Heteroaryl-3-Hydroxy-4H-Chromones: Synthesis, Spectral and Thermal Degradation Studies. *J Chinese Adv Mater Soc* **2013**, *1*, 257-267.
36. Karmakar, A.; Ambure, P.; Mallick, T.; Das, S.; Roy, K.; Begum, N.A. Exploration of Synthetic Antioxidant Flavonoid Analogs as Acetylcholinesterase Inhibitors: An Approach towards Finding Their Quantitative Structure–Activity Relationship. *Med Chem Res* **2019**, *28*, 723–741.
37. Xiong, W.; Wang, X.; Shen, X.; Hu, C.; Wang, X.; Wang, F.; Zhang, G.; Wang, C. Synthesis of Flavonols via Pyrrolidine Catalysis: Origins of the Selectivity for Flavonol versus Aurone. *J Org Chem* **2020**, *85*, 13160–13176.

38. Moffat, J.G.; Vincent, F.; Lee, J.A.; Eder, J.; Prunotto, M. Opportunities and Challenges in Phenotypic Drug Discovery: An Industry Perspective. *Nat Rev Drug Discov* **2017**, *16*, 531–543.
39. Olías-molero, A.I.; de la Fuente, C.; Cuquerella, M.; Torrado, J.J.; Alunda, J.M. Antileishmanial Drug Discovery and Development: Time to Reset the Model? *Microorganisms* **2021**, *9*, 2500.
40. Buxbaum, L.U.; Denise, H.; Coombs, G.H.; Alexander, J.; Mottram, J.C.; Scott, P. Cysteine Protease B of Leishmania Mexicana Inhibits Host Th1 Responses and Protective Immunity. *J Immunol* **2003**, *171*, 3711-3717.
41. Siqueira-Neto, J.L.; Debnath, A.; McCall, L.I.; Bernatchez, J.A.; Ndao, M.; Reed, S.L.; Rosenthal, P.J. Cysteine Proteases in Protozoan Parasites. *PLoS Negl Trop Dis* **2018**, *12*, e0006512.
42. Gontijo, V.S.; Judice, W.A.S.; Codonho, B.; Pereira, I.O.; Assis, D.M.; Januário, J.P.; Caroselli, E.E.; Juliano, M.A.; de Carvalho Dosatti, A.; Marques, M.J.; Viegas, Jr. C.V.; dos Santos, M.H. Leishmanicidal, Antiproteolytic and Antioxidant Evaluation of Natural Biflavonoids Isolated from Garcinia Brasiliensis and Their Semisynthetic Derivatives. *Eur J Med Chem* **2012**, *58*, 613-623.
43. Juliano, M.A.; Brooks, D.R.; Selzer, P.M.; Pandolfo, H.L.; Judice, W.A.S.; Juliano, L.; Meldal, M.; Sanderson, S.J.; Mottram, J.C.; Coombs, G.M. Differences in Substrate Specificities between Cysteine Protease CPB Isoforms of Leishmania Mexicana Are Mediated by a Few Amino Acid Changes. *Eur J Biochem* **2004,** *271*, 3704-3714.
44. Denise, H.; McNeil, K.; Brooks, D.R.; Alexander, J.; Coombs, G.H.; Mottram, J.C. Expression of Multiple CPB Genes Encoding Cysteine Proteases Is Required for Leishmania Mexicana Virulence in Vivo. *Infect Immun* **2003**, *71*, 3190–3195.
45. Raghav, N.; Kaur, R. Chalcones, Semicarbazones and Pyrazolines as Inhibitors of Cathepsins B, H and L. *Int J Biol Macromol* **2015**, *80*, 710-724.
46. Gomes, M.N.; Alcântara, L.M.; Neves, B.J.; Melo-Filho, C.C.; Freitas-Junior, L.H.; Moraes, C.B.; Ma, R.; Franzblau, S.G.; Muratov, E.; Andrade, C.H. Computer-Aided Discovery of Two Novel Chalcone-like Compounds Active and Selective against Leishmania Infantum. *Bioorg Med Chem Lett* **2017**, *27*, 2459-2464.
47. de Novais, L.M.R.; de Arueira, C.C.O.; Ferreira, L.F.; Ribeiro, T.A.N.; Sousa, P.T.; Jacinto, M.J.; de Carvalho, M.G.; Judice, W.A.S.; Jesus, L.O.P.; de Souza, A.A.; Torquato, H.F.V.; Parede-Gamero, E.J.; Silva, V.C. 4'-Hydroxy-6,7-Methylenedioxy-3-Methoxyflavone: A Novel Flavonoid from Dulacia Egleri with Potential Inhibitory Activity against Cathepsins B and L. *Fitoterapia* **2019**, *132*, 26-29.
48. Kerr, I.D.; Lee, J.H.; Farady, C.J.; Marion, R.; Rickert, M.; Sajid, M.; Pandey, K.C.; Caffrey, C.R.; Legac, J.; Hansell, E.; McKerrow, J.H.; Craik, C.S.; Rosenthal, P.J.; Brinen, L.S. Vinyl Sulfones as Antiparasitic Agents and a Structural Basis for Drug Design. *J Biol Chem* **2009**, *284*, 25697-25703.
49. Mendieta, L.; Picó, A.; Tarragó, T.; Teixidó, M.; Castillo, M.; Rafecas, L.; Moyano, A.; Giralt, E. Novel Peptidyl Aryl Vinyl Sulfones as Highly Potent and Selective Inhibitors of Cathepsins L and B. *ChemMedChem* **2010**, *5*, 1556-1557.
50. Brinen, L.S.; Hansell, E.; Cheng, J.; Roush, W.R.; McKerrow, J.H.; Fletterick, R.J. A Target within the Target: Probing Cruzain's P1' Site to Define Structural Determinants for the Chagas' Disease Protease. *Structure* **2000**, *8*, 831-840.
51. Freeman, A.M.; Mole, B.M.; Silversmith, R.E.; Bourret, R.B. Action at a Distance: Amino Acid Substitutions That Affect Binding of the Phosphorylated CheY Response Regulator and Catalysis of Dephosphorylation Can Be Far from the CheZ Phosphatase Active Site. *J Bacteriol* **2011**, *193*, 4709-4718.
52. Judice, W.A.S.; Mottram, J.C.; Coombs, G.H.; Juliano, M.A.; Juliano, L. Specific Negative Charges in Cysteine Protease Isoforms of Leishmania Mexicana Are Highly Influential on the Substrate Binding and Hydrolysis. *Mol Biochem Parasitol* **2005,** *144*, 36-43.
53. Santiago, A.S.; Pita, S.S. da R.; Guimarães, E.T. Tratamento Da Leishmaniose, Limitações Da Terapêutica Atual e a Necessidade de Novas Alternativas: Uma Revisão Narrativa. *Res Soc Dev* **2021**, *10*, e29510716543.
54. Cohen, A.; Azas, N. Challenges and Tools for in Vitro Leishmania Exploratory Screening in the Drug Development Process: An Updated Review. *Pathogens* **2021**, *10*, 1608.
55. Gupta, S.; Nishi, Visceral Leishmaniasis: Experimental Models for Drug Discovery. *Indian J Med Res* **2011**, *133*, 27–39.
56. Trefzger, O.S.; das Neves, A.R.; Barbosa, N. v.; Carvalho, D.B.; Pereira, I.C.; Perdomo, R.T.; Matos, M.F.C.; Yoshida, N.C.; Kato, M.J.; de Albuquerque, S.; Arruda, C.C.P.; Baroni, A.C.M. Design, Synthesis and Antitrypanosomatid Activities of 3,5-Diaryl-Isoxazole Analogues Based on Neolignans Veraguensin, Grandisin and Machilin G. *Chem Biol Drug Des* **2019**, *93*, 313-324.
57. Lipinski, C.A.; Lombardo, F.; Dominy, B.W.; Feeney, P.J. Experimental and Computational Approaches to Estimate Solubility and Permeability in Drug Discovery and Development Settings. *Adv Drug Deliv Rev* **1997**, *23*, 3-25.
58. Sander, T. OSIRIS Property Explorer. Organic Chemistry Portal 2001.
59. Daina, A.; Michielin, O.; Zoete, V. SwissADME: A Free Web Tool to Evaluate Pharmacokinetics, Drug-Likeness and Medicinal Chemistry Friendliness of Small Molecules. *Sci Rep* **2017**, *7*, 42717.
60. Perrin, D.D.; Armarego, W.L.F. Purification of Laboratory Chemicals; Pergamon Press, Oxford, 1988;
61. James J. P. Stewart, Stewart Computational Chemistry, Colorado Springs, CO, U. MOPAC2016.
62. Waterhouse, A.; Bertoni, M.; Bienert, S.; Studer, G.; Tauriello, G.; Gumienny, R.; Heer, F.T.; de Beer, T.A.P.; Rempfer, C.; Bordoli, L.; Lepore, R.; Schwede, T. SWISS-MODEL: Homology Modelling of Protein Structures and Complexes. *Nucleic Acids Res* **2018**, *46*, W296-W303
63. Pettersen, E.F.; Goddard, T.D.; Huang, C.C.; Couch, G.S.; Greenblatt, D.M.; Meng, E.C.; Ferrin, T.E. UCSF Chimera--a Visualization System for Exploratory Research and Analysis. *J Comput Chem* **2004**, *25*, 1605–1612.
64. Spoel, D.V.D.; Lindahl, E.; Hess, B.; Groenhof, G.; Mark, A.E.; Berendsen, H.J.C. GROMACS: Fast, Flexible, and Free. *J Comput Chem* **2005**, *26*, 1701–1718.

 doi:10.20944/preprints202211.0376.v1

65. Vanommeslaeghe, K.; Hatcher, E.; Acharya, C.; Kundu,S.; Zhong,S.; Shim, J.; Darian, E.; Guvench, O.; Lopes, P.; Vorobyov, I.; Mackerell Jr. A.D. CHARMM General Force Field: A Force Field for Drug-like Molecules Compatible with the CHARMM All-atom Additive Biological Force Fields. *J Comput Chem* **2010**, *31*, 671–690.
66. Zoete, V.; Cuendet, M.A.; Grosdidier, A.; Olivier Michielin SwissParam: A Fast Force Field Generation Tool ForSmall Organic Molecules. *J Comput Chem* **2011**, *32*, 2359–2368.
67. Skehan, P.; Storeng, R.; Scudiero, D.; Monks, A.; Mcmahon, J.; Vistica, D.; Warren, J.T.; Bokesch, H.; Kenney, S.; Boyd, M.R. New Colorimetric Cytotoxicity Assay for Anticancer-Drug Screening. *J Natl Cancer Inst* **1990**, *82*, 1107-1112.
68. Monks, A.; Scudiero, D.; Skehan, P.; Shoemaker, R.; Paull, K.; Vistica, D.; Hose, C.; Langley, J.; Cronise, P.; Vaigro-wolff, A.; Gray-Goodrich, M.; Campbell, H.; Mayo, J.; Boyd, M. Feasibility of a High-Flux Anticancer Drug Screen Using a Diverse Panel of Cultured Human Tumor Cell Lines. *J Natl Cancer Inst* **1991**, *11*, 757-66.